Ocean Engineering 317 (2025) 120060

Contents lists available at ScienceDirect

Ocean Engineering

journal homepage: www.elsevier.com/locate/oceaneng

Research paper

Numerical and experimental investigation of motion characteristics of a travelling trimaran encountering a freak wave

Zhen Liu [a], Haipeng Zhang [a], Lei Shi [a], Kaiyuan Shi [b], Gang Chen [a], Longbin Tao [c,d,*]

[a] Shanghai Key Laboratory of Ship Engineering, Marine Design and Research Institute of China, Shanghai, 200011, China
[b] School of Naval Architecture, Ocean and Civil Engineering, Shanghai Jiao Tong University, Shanghai, 200240, China
[c] College of Harbour, Coastal and Offshore Engineering, Hohai University, 1 Xikang Road, Nanjing, 210098, China
[d] Department of Naval Architecture, Ocean and Marine Engineering, University of Strathclyde, Glasgow, G40LZ, United Kingdom

ARTICLE INFO

Keywords:
Trimaran
Model test
Motion characteristic
Freak wave
Rogue wave

ABSTRACT

A hybrid frequency-time domain model has been developed to investigate motion characteristics of a travelling trimaran encountering a freak wave. A deterministic wave train containing a freak wave was modelled in a towing tank at Marine Design and Research Institute of China for testing the model trimaran under the action of the freak wave. Comprehensive numerical simulations examine the effect of the encountering position of the trimaran with the freak wave, forward speed and the configuration of side hulls on heave and pitch motions of the trimaran excited by the freak wave. It is found that there exists a feature of phase leading of the heave and pitch time histories around the occurrence time of the freak wave as the encountering position moves astern. It is further demonstrated that different encountering positions of the trimaran with the freak wave crest can merely lead to slight difference for the maximum peak-trough values of the heave and pitch motions, respectively. The maximum peak-trough values of the heave and pitch motion of the trimaran encountering the freak wave crest with center of gravity (CG) at different forward speeds tend to increase and decrease respectively as the forward speed increases. The time history of pitch motion is found to exhibit a whole downshift as the side hulls move forward.

1. Introduction

In the field of high-speed vessels (Faltinsen, 2005), trimarans have received more and more attentions due to their excellent hydrodynamic performance. Trimarans consist of one large main (center) hull with two smaller side (outrigger) hulls. The main hull is crucial to determine the hydrodynamic performance, and usually relatively slender and can reduce the vessel's wave resistance. The side hulls mainly play a key role in improving seakeeping and stability. Due to different layouts of side hulls of trimarans, it is of primary significance to study the effect of side-hull layouts on seakeeping performance of trimarans.

Over the past decades, considerable efforts have been made to investigate the influence of side-hull layouts of trimarans on seakeeping performance. Hebblewhite et al. (2007) investigated the influences of the longitudinal spacing of the side hulls of a trimaran on the heave and pitch motion performance. They found that the heave and pitch response magnitudes decrease respectively as the side hulls move astern. It was also pointed out that the tendency could be due to either the increase in the pitch radius of gyration associated with the backward movement of side hulls or the different hydrodynamic interference characteristics for each layout of longitudinal spacings. By means of 3D pulsating source method, Fang and Too (2006) studied the influence of side-hull layouts on the heave and pitch motions of a trimaran ship travelling in regular waves. It was indicated that the trimaran arrangement with smaller longitudinal spacing and larger transverse spacing is generally more advantageous in consideration of seakeeping performance. Based on 2.5D potential theory, Wei (2007) studied the characteristic of hydrodynamic interference between the hulls of a trimaran, and the effect of the stagger and transverse spacing on the hydrodynamic coefficients and diffraction force. It was found that 2.5D theory can give satisfactory predictions of the motion response characteristics of the trimaran.

Based on linear theory, Fang and Chen (2008) calculated the wave loads on a trimaran ship travelling in irregular waves to select appropriate side-hull layouts. Deng et al. (2019) investigated the resistance in still water, added resistance and motion response of a trimaran in regular head waves with different wave amplitudes by CFD method. It was

* Corresponding author. College of Harbour, Coastal and Offshore Engineering, Hohai University, 1 Xikang Road, Nanjing, 210098, China.
E-mail address: longbin.tao@hhu.edu.cn (L. Tao).

https://doi.org/10.1016/j.oceaneng.2024.120060
Received 4 September 2024; Received in revised form 23 November 2024; Accepted 7 December 2024
0029-8018/© 2024 The Authors. Published by Elsevier Ltd. This is an open access article under the CC BY license (http://creativecommons.org/licenses/by/4.0/).

indicated that the added resistance triggered by the main hull dominates the total added resistance and decreases as wave amplitude decreases.

Gong et al. (2020) numerically investigated added resistance and motion characteristics of a trimaran in oblique waves by a hybrid method which combine the fully nonlinear potential flow theory and viscous flow theory, and the influence of side-hull layout on the motion performance of a trimaran in different wave headings was further analyzed by Gong et al. (2021). It was found the stagger of the side hulls has a noticeable influence on the motion performance of the trimaran. Duan et al. (2019) investigated the heave and pitch motions and added resistance of a trimaran in head waves by 2.5D method and model test, respectively. The effect of forward speed, side-hull position, incident waves on the motion response and added resistance of the trimaran was analyzed in depth. Tang et al. (2020) studied the motion and wave load characteristics of a trimaran in small heeling condition by model test and numerical simulations, respectively. It was revealed that in small heeling condition the heave motion of the trimaran appears to be milder while the pitch and roll motions increase significantly in comparison to the trimaran with side-hull layout at stern. By means of a 3D panel method, Yao et al. (2023) numerically investigate the motion performance and added resistance of a trimaran advancing in waves, and the influence of side-hull position on the motion response, added resistance and interference effect were analyzed in depth. Zhang et al. (2023) investigated the influence of a novel anti-rolling hydrofoil on roll damping and roll motion by CFD method and 3D potential flow theory, respectively. It was demonstrated the hydrofoils with four schemes possess high anti-rolling efficiency for a trimaran ship.

The aforementioned studies mainly focus on seakeeping performance of trimarans in regular waves and general irregular waves. With frequent occurrences of extreme marine environments in recent decades, more and more attentions have been paid to the navigation and operation safety of ships and offshore structures in freak waves. Freak waves, also known as rogue waves or giant waves are transient and extremely large waves. Presently, no unified definition of freak waves has been established, but one extensively accepted definition takes for a freak wave to be a wave whose height exceeding at least twice the significant wave height (Kharif et al., 2008). Freak waves can result in huge damage to ships and offshore structures. Over the past several years, many accidents related to impact of freak waves on sailing ships or offshore platforms have been reported (Bertotti and Cavaleri, 2008; Haver and Andersen, 2000; Kharif et al., 2008). In recent decades, many researchers studied the interaction of freak waves with ships and offshore platforms. Guedes Soares et al. (2005) investigated experimentally and numerically the motion response and wave loads of an FPSO induced by a freak wave. It was shown that the numerical model in the framework of time-domain nonlinear strip theory could give satisfactory prediction on the bending moment at midship for the ship in a strongly nonlinear wave. Clauss and Klein (2011) carried out an experimental study on the motion and wave load characteristics of a Ro-Ro ship in the well-known freak wave, i.e. "New Year Wave''. It is revealed that the rogue wave impact on the ship is rigorous and results in significant global loads. Bennett et al. (2013) investigated the effect of travelling speed on the motion response of a frigate ship in freak waves by numerical method and model test, respectively. It is demonstrated that the magnitude of heave motion response increases with increased travelling speed, while the magnitude of the pitch motion response decreases at higher speeds. Zhang et al. (2022) performed numerical simulations on the encountering of an LNG-carrier with three deterministic focused waves produced by linear and nonlinear physical mechanisms, respectively. It was found that the focal position and incident angle could lead to distinct discrepancy for the motion response peaks by linear and nonlinear focused waves. Colagrossi et al. (2001) developed a time domain potential flow model based on a Rankine panel method for linearized ship seakeeping, and calculated the motion response of a Wigley trimaran under a transient wave packet. It was indicated that the motion RAOs of the trimaran ship based on time domain analysis are in good agreement with corresponding experimental measurements.

In terms of ship motion simulation, a hybrid frequency-time domain method can balance efficiency and accuracy especially for motion prediction of ships in rough seas, which has been widely used in recent years. Begovic et al. (2020) developed a hybrid frequency-time domain program based on Hydrostar to assess the vertical motions of hard chine displacement hull. Pennino and Scamardella (2023) developed a hybrid frequency-time domain motion simulation program for a research ship based on the open-source NEMOH code. The effectiveness of the code has been validated by the onboard measurements. By means of LaiDyn, a frequency-time domain motion simulation code that can consider propeller actions, Acanfora et al. (2017) investigated large amplitude motions and the associated longitudinal and transverse accelerations of a container ship in heavy weather.

To date, the literature on the impact of a freak wave on a travelling trimaran is still rather limited. The influences of encountering position, forward speed and side-hull configuration on the motion response characteristics of a travelling trimaran encountering a freak wave need to be investigated in depth. This study develops a hybrid frequency-time domain model to investigate motion characteristics of a trimaran encountering a freak wave. In order to validate the numerical model, a deterministic wave train containing a freak wave was modelled in a towing tank at Marine Design and Research Institute of China (MARIC) to carry out the model test of the trimaran under the action of the freak wave. The deterministic wave train containing a freak wave measured in the test was reconstructed in numerical simulations to study the effect of the encountering position of the trimaran with the freak wave, the forward speed and the side-hull configuration on heave and pitch motions of the trimaran under the action of the freak wave. The present paper is organized as follows. The details of the hybrid frequency-time domain model for ship motions are described in Section 2 following Introduction. The experimental approach and setup of the model test are introduced in Section 3. The detailed results and discussion on the validation of the numerical model as well as the influences of encountering position, forward speed and side-hull configuration on the motion response characteristics of a travelling trimaran encountering a freak wave are given in Section 4. At last, the conclusions are drawn in Section 5.

2. Hybrid frequency-time domain model for ship motions

The hybrid frequency-time domain model is based on the impulse response functions (IRFs) obtained by means of linear frequency domain analysis results of radiation and diffraction forces and moments on a ship below the mean waterline. The frequency domain added mass and radiation damping coefficients are utilized to calculate the radiation IRF. Then, the radiation wave forces in time domain can be obtained by convolution integral representation of the corresponding IRF. The diffraction wave forces in time domain are also calculated by convolution integral representation of the IRF obtained based on frequency domain diffraction wave forces. Further, a time domain simulation of ship motions in wave is performed considering nonlinear incident wave (Froude–Krylov) and restoring forces and moments by integrating the pressures at each time step over the exact undisturbed instantaneous wetted surface of the ship, which requires a full mesh model, i.e. the mesh division of the ship to the upper deck level. The instantaneous wetted surface is obtained by tracking the interface between the incident wave and the full mesh model at each time step. The fourth-order Runge-Kutta method is used to solve the time-domain equations, and a simulation program was developed using the Fortran 95. The added mass and radiation damping coefficients in frequency domain are computed by means of a program developed by our team based on a translating-pulsating Green function in framework of 3D potential theory. The validation of the effectiveness of program can be found in the reference (Liang et al., 2016). The details of the hybrid frequency-time domain model are elaborated as follows.

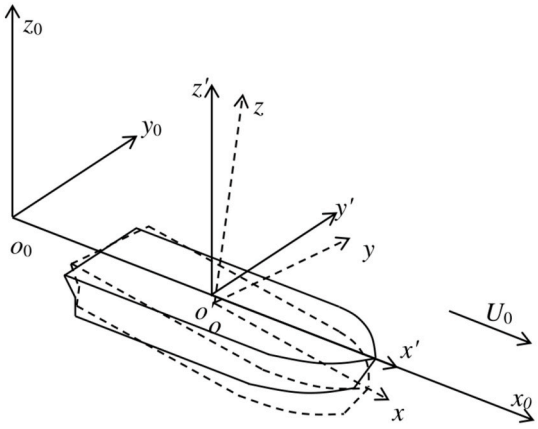

Fig. 1. Coordinate systems in the numerical model.

2.1. Theoretical formulation

In order to describe ship motions in waves, three different coordinate systems are introduced, as shown in Fig. 1. The coordinate system $o_0x_0y_0z_0$ is a spatial fixed coordinate system, which is fixed in the flow field with x_0-axis pointing positive to the bow and with z_0-axis pointing positive upwards, coinciding with the still water free surface. This coordinate system facilitates the expression of incident waves. The coordinate system $o'x'y'z'$ is the reference coordinate system advancing at the ship forward speed U_0 with $o'x'y'$ plane coinciding with the still water level, the origin o' located amidship and z'-axis positive upwards. These two coordinate systems coincide at the initial moment when $t = 0$. The coordinate system $oxyz$ is fixed on the hull, translating and rotating with the ship. When the ship is in equilibrium, it completely coincides with the reference coordinate system.

2.2. Calculation of radiation wave forces

Following Cummins (1962), the radiation forces in the hull-fixed coordinate system are evaluated by

$$F_{kj}^R(t) = -\mu_{kj}\ddot{\xi}_j(t) - b_{kj}\dot{\xi}_j(t) - c_{kj}\xi_j(t) - \int_0^t K_{kj}(t-\tau)\dot{\xi}_j(\tau)d\tau \tag{1}$$

where F_{kj}^R denotes the k-direction radiation force induced by j-mode radiation motion. $\xi_j(t)$, $\dot{\xi}_j(t)$, $\ddot{\xi}_j(t)$, $j = 1, 2, \cdots 6$ mean motion displacement, velocity and acceleration of j-mode of the oscillation, respectively. μ_{kj} represents the added mass coefficients at infinite frequency and merely relies on the ship geometry under the mean wetted water surface. b_{kj} and c_{kj} represent the damping and restoring force coefficients at infinite frequency and depend on hull geometry underwater and travelling speed, which are perceived as a rectification to the radiation forces due to forward speed induced steady flow around the ship. $K_{kj}(t)$ refers to the retardation function which is associated with the hull geometry underwater, forward speed and time, and reflects the fluid response memory effect and should be calculated at each time step.

Assuming the ship is in harmonic motion of a certain mode defined by $e^{-i\omega t}$ and the flow field has reached steady state, Eq. (1) can be derived as

$$F_{kj}^R(t) = \left[\omega^2\mu_{kj} + i\omega b_{kj} - c_{kj} + \int_0^\infty d\tau i\omega e^{i\omega\tau}K_{kj}(\tau)\right]e^{-i\omega t} \tag{2}$$

According to frequency domain theory, the harmonic radiation forces can be described using frequency-domain added-mass A_{kj} and damping coefficients B_{kj} as

$$F_{kj}^R(t) = \left[\omega^2 A_{kj}(\omega) + i\omega B_{kj}(\omega)\right]e^{-i\omega t} \tag{3}$$

Comparing related terms in Eqs. (2) and (3), the following relations can be derived

$$A_{kj}(\omega) = \mu_{kj} - \frac{1}{\omega}\int_0^\infty K_{kj}(t)sin(\omega t)dt - \frac{c_{kj}}{\omega^2} \tag{4}$$

$$B_{kj}(\omega) = b_{kj} + \int_0^\infty K_{kj}(t)cos(\omega t)dt \tag{5}$$

Eqs. (4) and (5) give the relationship between the retardation function and frequency-domain hydrodynamic coefficients. Then the retardation function can be obtained by inverse fast Fourier transform (IFFT) of Eqs. (4) and (5) as follows

$$\begin{aligned} K_{kj}(t) &= \frac{2}{\pi}\int_0^\infty \left(B_{kj}(\omega) - b_{kj}\right)cos(\omega t)d\omega \\ K_{kj}(t) &= \frac{2}{\pi}\int_0^\infty \omega\left(\mu_{kj} - A_{kj}(\omega) - \frac{c_{kj}}{\omega^2}\right)sin\,\omega t d\omega \end{aligned} \tag{6}$$

According to King (1987), the b_{kj} should be equal to infinite frequency damping coefficients. In terms of Kramers-Kronig relation,

$$\begin{cases} c_{55} = -U_0^2\mu_{33}; c_{56} = U_0^2\mu_{32}; c_{65} = U_0^2\mu_{23}; c_{66} = -U_0^2\mu_{22} \\ c_{kj} = 0, k, j \neq 5; k, j \neq 6 \end{cases} \tag{7}$$

2.3. Calculation of incident wave forces

The incident wave forces/moments are computed by integrating the pressure at each time step over the exact undisturbed instantaneous wetted surface (S_b) of the ship. The instantaneous wetted surface is acquired by means of intersecting the instantaneous wave surface with the hull profile considering the motions of the ship at each time step. The incident wave force is calculated by

$$F_{k0}(t) = \iint_{S_b} p_I \bullet n_k ds \tag{8}$$

The incident wave pressure p_I is herein defined by linear dynamic pressure as

$$p_I = -\rho\frac{\partial\Phi_I}{\partial t} \tag{9}$$

2.4. Calculation of diffraction wave forces

The diffraction wave forces represent the interference effects resulting from the presence of the ship in the incident wave field. In linear diffraction problem, the instantaneous wave elevation is assumed to be composed of a series of impulses, and then the diffraction wave forces can be evaluated by

$$F_{k7}(t) = \int_{-\infty}^\infty K_{k7}(t-\tau)\zeta(\tau)d\tau, k = 1, 2, \cdots, 6 \tag{10}$$

where K_{k7} is the impulse response function for the k th mode diffraction force and ζ is the time history of wave elevation at the amidship where the origin of the reference coordinate system lies. Similar to the approach for solving radiation forces, assuming that the instantaneous wave surface elevation changes harmonically at a certain frequency in the reference coordinate system, we can obtain

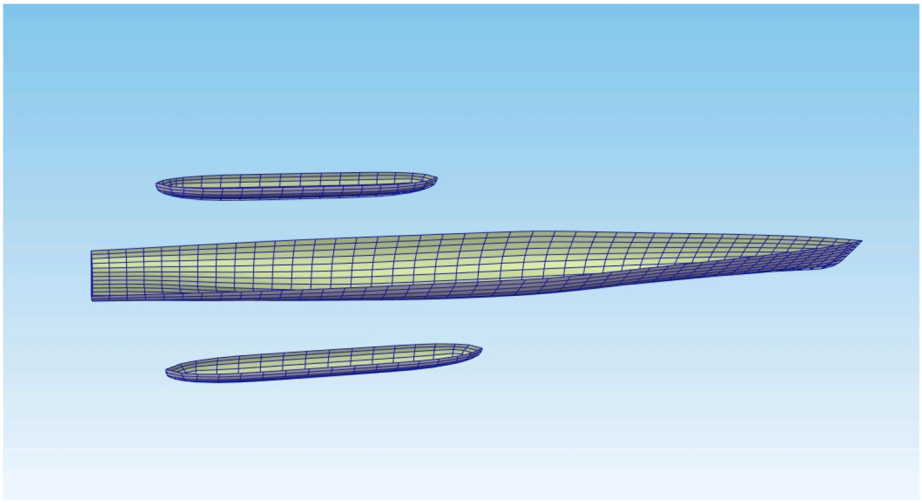

Fig. 2. The mesh model for frequency domain analysis.

$$Re[F_{k7}(\omega_e)] = \int_{-\infty}^{\infty} cos(\omega_e t)K_{k7}(t)dt \tag{11}$$

$$Im[F_{k7}(\omega_e)] = \int_{-\infty}^{\infty} sin(\omega_e t)K_{k7}(t)dt \tag{12}$$

Where ω_e refers to encounter frequency and can be given by $\omega_e = \omega - \kappa U_0 \cos\beta$, in which ω represents wave frequency, κ wave number, β incident wave angle. By means of IFFT based on Eqs. (11) and (12), the impulse response function can be expressed as

$$K_{k7}(t) = \frac{1}{\pi}\int_0^{\infty} \{Re[F_{k7}(\omega_e)]cos\ \omega_e t + Im[F_{k7}(\omega_e)]sin\ \omega_e t\}d\omega_e \tag{13}$$

2.5. Ship motion equations

In terms of Newton's second law, the 6 degrees of freedom (DoF) motion equations for a ship in waves can be derived as

$$\sum_{j=1}^{6}\left\{\left(M_{kj}+\mu_{kj}\right)\dot{\xi}_j(t) + \int_0^t K_{kj}(t-\tau)\dot{\xi}_j(\tau)d\tau + b_{kj}\dot{\xi}_j(t) + c_{kj}\xi_j(t)\right\} = F_{k0}(t) + F_{C_k}(t) + \int_{-\infty}^{\infty} K_{k7}(t-\tau)\zeta(\tau)d\tau, k = 1,2,\cdots,6 \tag{14}$$

where M_{kj} represents the generalized inertia matrix, F_{C_k} represents the restoring forces/moments and calculated by integrating the pressure over the undisturbed instantaneous wetted surface of the ship through

$$F_{C_k}(t) = -\iint_{S_b} \rho g z \bullet n_k ds \tag{15}$$

2.6. Numerical implementation of freak waves

In simulation of general irregular seas, the phases are randomly generated. In this study, to compare numerically calculated motion time histories with experimentally measured motion time histories, the accurate phase of each component wave of the freak wave train measured in experiment was obtained by fast Fourier transform (FFT). Then, the phase of each wave component could be converted to the origin of the spatial fixed coordinate system $o_0x_0y_0z_0$ according to the distance between the initial location (o_0) and the encountering location of the trimaran with the freak wave. To compare numerical simulation results

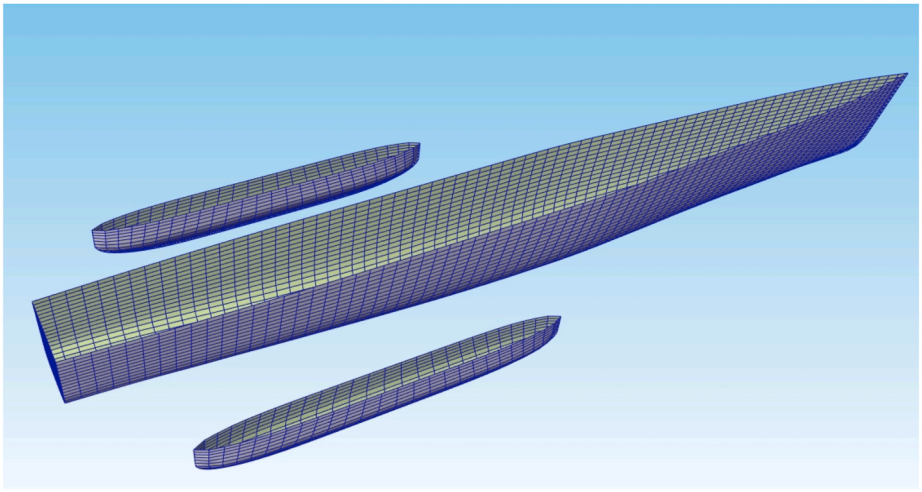

Fig. 3. The mesh model for time domain simulation.

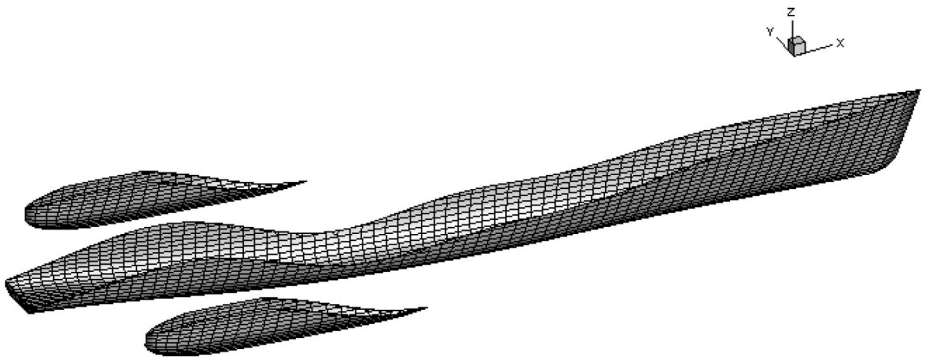

Fig. 4. The typical underwater mesh model for time domain simulation.

with experimental measurements, the first step is to reconstruct in numerical simulation the time history of wave elevation containing a freak wave measured at a specified location in the experiment, and ensure that the ship sailing at a certain forward speed can encounter the crest of the freak wave at the location. The target wave train containing a freak wave can be expressed as

$$\eta(t) = \sum_{n=1}^{N} a_n \cos(\omega_n t + \theta_n) \tag{16}$$

Where N, ω_n, a_n, θ_n denote the number, circular frequency, amplitude and phase of component wave, respectively. These coefficients can be obtained using FFT. The location of the encountering between the ship and the freak wave crest in the fixed coordinate system $x = x_c = U_0 t_c$, where t_c and x_c denote the occurrence time and position of the freak wave crest, then Eq (16) can be rewritten as

$$\eta(x_c, t) = \sum_{n=1}^{N} a_n \cos(\kappa_n x_c - \omega_n t - \varepsilon_n) \tag{17}$$

where $\varepsilon_n = \theta_n + \kappa_n x_c$.

Therefore, the time history of wave elevation at the initial position of the ship's center of gravity (CG) in the fixed coordinate system $x = x_0$ can be expressed as

$$\eta(x_0, t) = \sum_{n=1}^{N} a_n \cos(\kappa_n x_0 - \omega_n t - \varepsilon_n) \tag{18}$$

By utilizing the frequency, amplitude, and phase information provided by Eq. (18) in the numerical model, it can be achieved that the ship encounters a freak wave crest at U_0 at the position $x = x_c$ and time $t = t_c$.

2.7. Mesh settings

The mesh models were obtained with the commercial software *Gambit*. In order to balance accuracy and efficiency in the simulations, the number of mesh should be reasonably selected. In this study, the numbers of mesh based on frequency domain analysis and time domain simulation are determined as 1034 and 4615 respectively in terms of experience of mesh independence analysis. Figs. 2 and 3 show the mesh model for frequency domain analysis and time domain simulation, respectively. During the time-domain numerical simulation process, as the incident wave changes, the program can automatically cut the original mesh to obtain the underwater mesh. Fig. 4 shows the typical underwater mesh model for time domain simulation.

3. Model test

To validate the numerical model, a deterministic wave train containing a freak wave was modelled in a towing tank at MARIC to carry out model test of a trimaran under the action of a freak wave.

Table 1
Main particulars of the trimaran model.

Item	Unit	Trimaran model	
		Main hull	Side hull
L_{OA}	m	3.056	1.036
L_{WL}	m	2.944	1.031
L_{PP}	m	2.944	1.031
B_{WL}	m	0.228	0.068
T_F	m	0.169	0.099
T_A	m	0.169	0.099
∇_T	m^3	0.0699	
LCG (from aft perpendicular)	m	1.3278	
VCG (from baseline)	m	0.26	
R_{xx}	m	0.1889	
R_{yy}	m	0.8056	

Table 2
Layout scheme of the trimaran model.

	L_h (m)	B_h (m)
L1B1	0.736	0.41
L1B2	0.736	0.55
L1B3	0.736	0.69
L2B1	0.458	0.41
L3B1	0.178	0.41

3.1. Experimental setup

The experiment was conducted in a towing tank with a maximum carriage speed of 9 m/s. The dimension of the tank is 280 m × 10 m × 5 m. A flap-type wavemaker is installed at one end in the tank to generate regular or irregular waves, and a slope-type absorber is installed at the other end to absorb incident waves and eliminate influences of wave reflection. According to the capacity of the wave-maker and weight control requirements of a ship model, the scale ratio of the tested trimaran model is selected as 18 that satisfies the requirement of geometric similarity. The trimaran model was adjusted on a trimming table to guarantee the correct properties, including the mass, the center of gravity and the inertia radius of gyration. The main particulars of the trimaran model are provided in Table 1.

In numerical simulations, different configurations of the trimaran shown in Table 2 are taken into account to study the influence of stagger and transverse spacing on the motion characteristics of the trimaran under a freak wave. Longitudinal stagger L_h and transverse spacing B_h of the configurations are defined in Fig. 5. In order to validate the numerical model, experiments associated with a freak wave based on the L1B1 configuration were carried out. Fig. 6 shows the snapshot of the trimaran model with L1B1 configuration. The trimaran model was

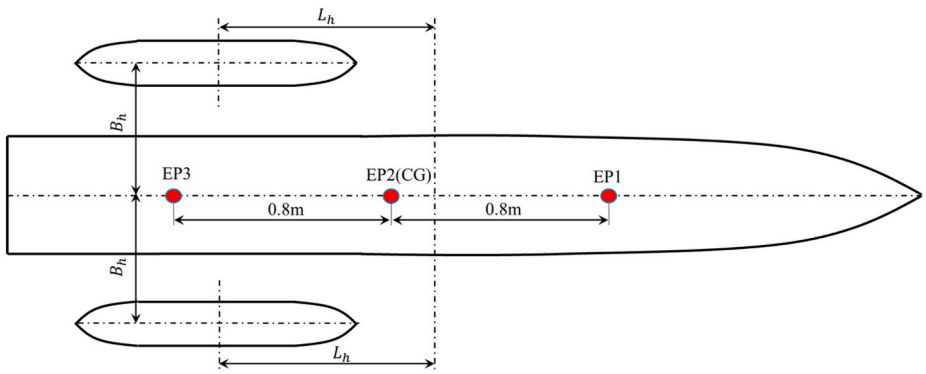

Fig. 5. Schematic diagram of the layout of the trimaran.

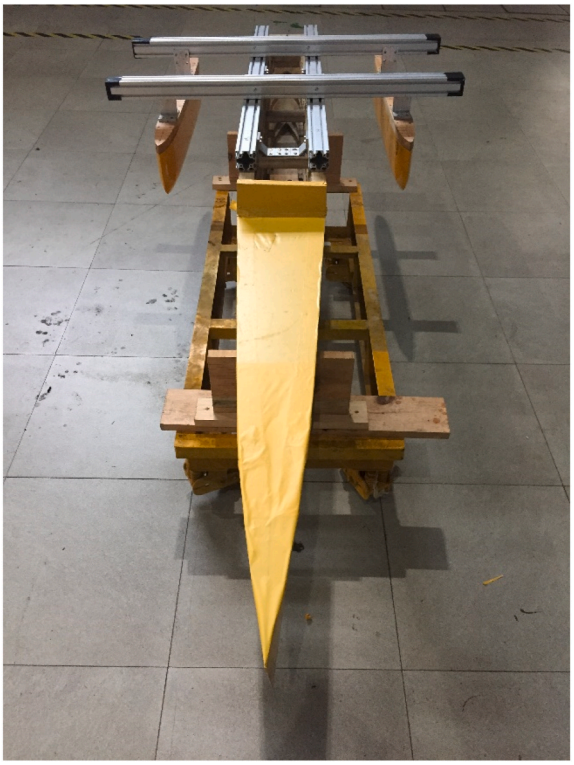

Fig. 6. The snapshot of the trimaran model (L1B1).

connected to a seaworthiness instrument (see Fig. 8) and can be towed with heave and pitch degrees of freedom in head waves at a given forward speed. The heave and pitch motions were measured using the seaworthiness instrument. A wave probe was placed at a specific position to measure the time history of freak wave before towing tests. The sampling frequency in the experiment is 50Hz. Fig. 7 shows the schematic diagram of the model test. Fig. 8 shows the snapshot of the trimaran model with L1B1 configuration encountering a freak wave at a forward speed $V_m = 1.2$ m/s in the model test.

3.2. Simulation of freak waves

In this study, a target wave train containing a freak wave is designed with the double wave train model (Kriebel and Alsina, 2000), i.e., constructing a freak wave train by linear superposition of a focusing wave train and a background random wave train. Then the target wave train is reproduced at a specified location of the towing tank by means of linear superposition principal and the phase backward propagation technique (Yu, 2003) to conduct the model test. Fig. 9 shows the time history of the freak wave train experimentally measured with a fixed wave probe far from the wavemaker 50m (see Fig. 7) in the test. The significant wave height (H_s) of the measured wave train is 0.11m corresponding to a moderate (4-band) sea state in prototype scale. It can be seen that the measured maximum wave height (H_{max}) around the time instant of 60s is approximately 0.26m which is nearly 2.2 times the significant wave height (0.11m). This means that the experimentally measured maximum wave height satisfies the engineering definition of freak waves, i.e. $H_{max}>2H_s$ (Kharif and Pelinovsky, 2003).

3.3. Freak wave tests

The seakeeping tests of the trimaran model towed in head wave condition at a specified forward speed to encounter the freak wave are carried out in the towing tank. During the test, a computer controls wave-making and records testing data. Before the test of the trimaran model encountering the freak wave, it is necessary to determine the distance between the starting position of the model and the occurrence

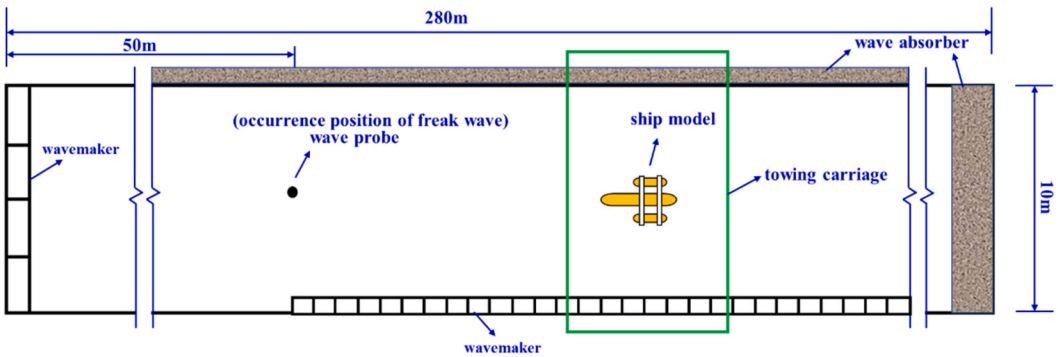

Fig. 7. Schematic diagram of the model test (Top view).

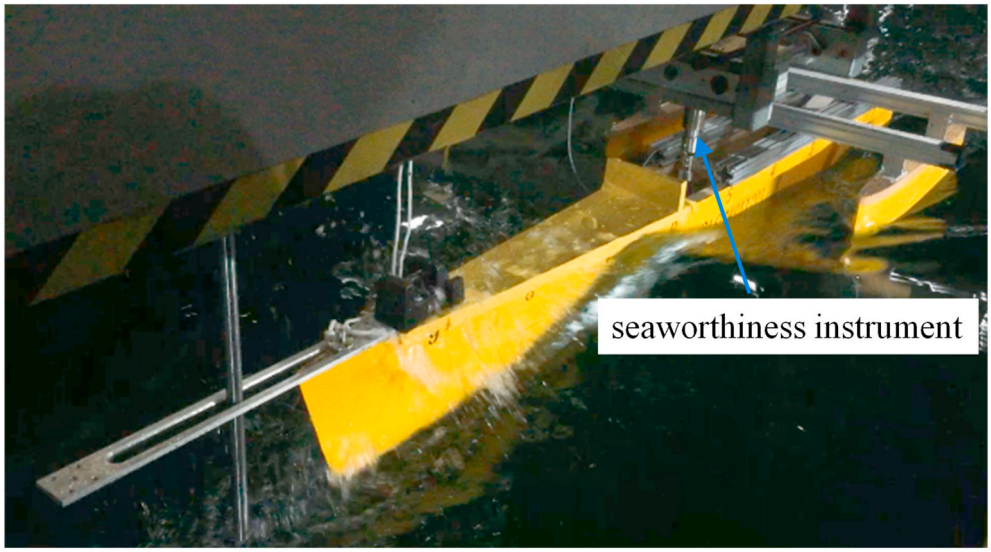

Fig. 8. The snapshot of the trimaran model with L1B1 configuration encountering a freak wave at $V_m = 1.2$ m/s in the model test.

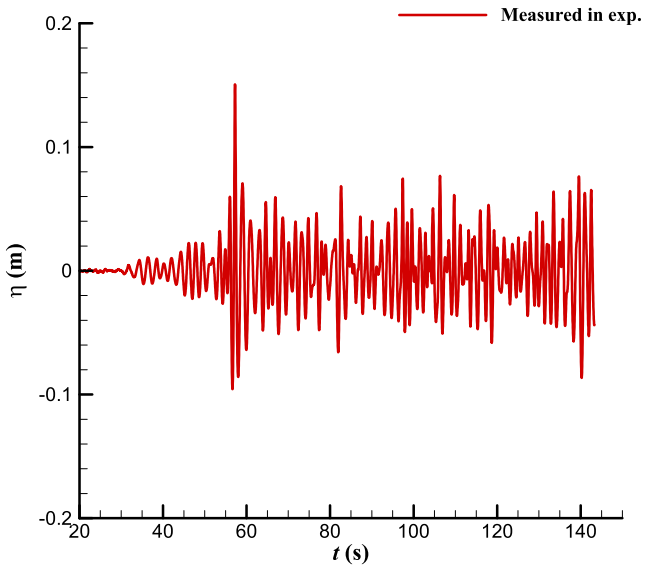

Fig. 9. The time history of the freak wave train measured with a fixed wave probe in the test.

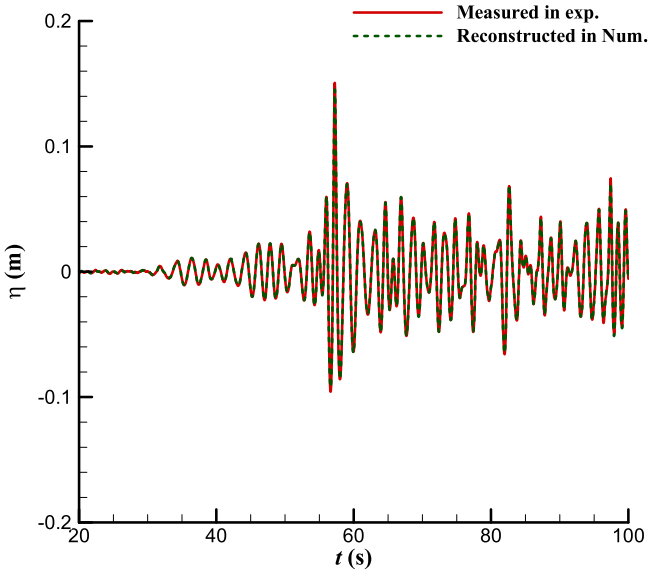

Fig. 10. Comparison between the deterministic wave train containing a freak wave measured at a fixed point in the experiment and corresponding numerical reconstruction.

position of the freak wave in the towing tank according to the forward speed of the trimaran model and occurrence time of the freak wave. Then it is ensured that the towed trimaran model can encounter the freak wave at the occurrence position.

4. Results and discussion

4.1. Validation of numerical model

In order to validate the numerical model, the experimentally measured deterministic wave train containing a freak wave was reconstructed in the numerical model to simulate the freak wave action on the trimaran. Fig. 10 shows the comparison between the deterministic wave train containing a freak wave measured at a fixed point in the experiment and corresponding numerical reconstruction. It can be clearly seen that the agreement between the numerical reconstruction and the measured wave train is rather satisfactory.

Figs. 11 and 12 show the comparison of the time histories of the heave and pitch motion of the trimaran encountering the freak wave at $V_m = 1.2$ m/s measured in the experiment and calculated by numerical simulation, respectively. It is seen that the phase agreement of the time history of the heave motion is acceptable. It is noted that the peaks and troughs of the heave and pitch motion around the occurrence time (60s) of the freak wave by numerical simulation are relatively significantly higher than those measured in the experiment. This is mainly due to the greater damping effect induced by the ship model seaworthiness instrument especially when the motion of the trimaran is pronounced.

4.2. Effect of encountering position

In order to investigate the effect of the encountering position of the trimaran with the freak wave crest on the motion response, the occurrence time of the freak wave crest is set at $t = 60$s with different encountering positions (EP), i.e. EP1, EP2 and EP3 (see Fig. 5) of the trimaran in the numerical simulations. The simulations are based on

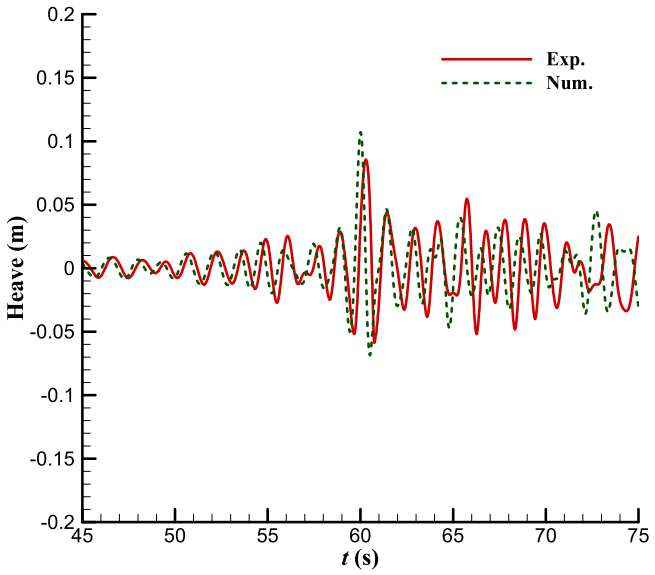

Fig. 11. Comparison between the experimental measurements and numerical results of the time histories of the heave motion of the trimaran encountering a freak wave at $V_m = 1.2$ m/s.

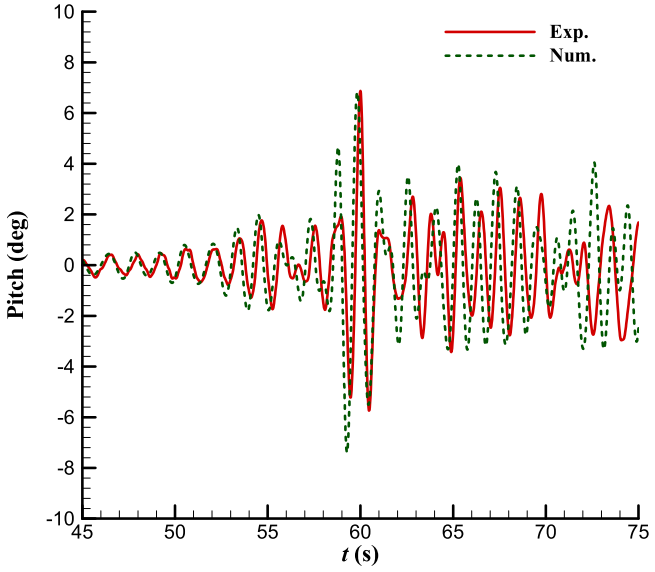

Fig. 12. Comparison between the experimental measurements and numerical results of the time histories of the pitch motion of the trimaran encountering a freak wave at $V_m = 1.2$ m/s.

L1B1 layout of the trimaran. Figs. 13 and 14 show the comparison of the time histories of the heave and pitch motion between different encountering positions of the trimaran at $V_m = 1.2$ m/s with the freak wave crest, respectively. It can be seen in Figs. 13 and 14 that there exist two larger peak values and one larger trough value ranging from 60s to 62s after the action of the freak wave crest on different positions of the trimaran. The more ahead the action position of the freak wave crest, the later the time of the occurrence of the heave and pitch peaks and troughs. This is due to when the encountering position near the stern of the trimaran, during the propagation and evolution process of the freak wave crest before approaching the encountering position, the undeveloped freak wave crest has already begun to lead to significant disturbances on the trimaran hull. To see the influence of the encountering position on the intensity of the heave and pitch motion in the freak wave, the comparison of the maximum peak-trough values of the heave

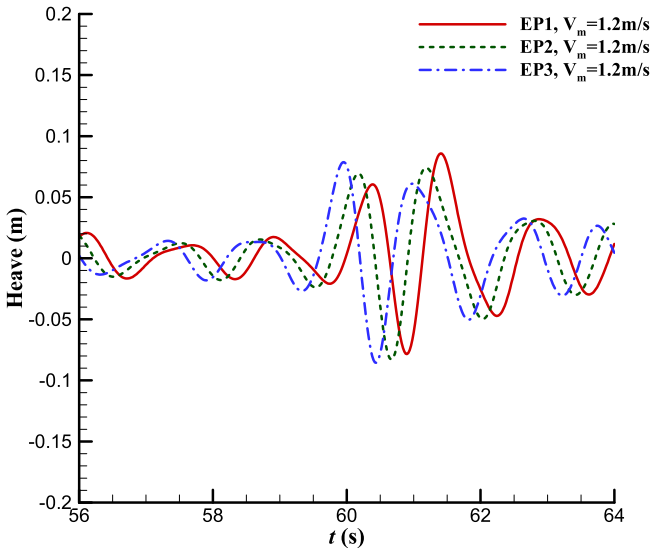

Fig. 13. Comparison of the time histories of the heave motion of the trimaran encountering the freak wave with different positions at $V_m = 1.2$ m/s.

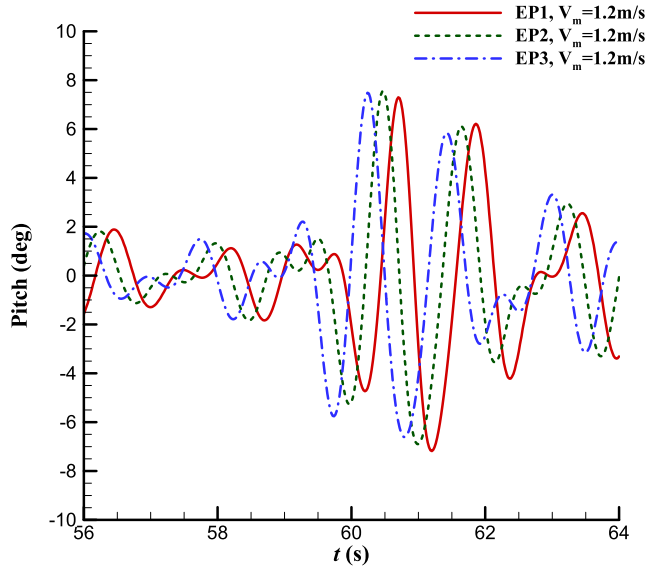

Fig. 14. Comparison of the time histories of the pitch motion of the trimaran encountering the freak wave with different positions at $V_m = 1.2$ m/s.

Table 3
Maximum peak-trough values of the heave and pitch time histories of the trimaran encountering the freak wave with different positions at $V_m = 1.2$ m/s.

Encountering position	Heave (m)	Pitch (deg)
EP1	0.1643	14.48
EP2	0.1571	14.45
EP3	0.1644	14.1

and pitch time histories are shown in Table 3. It can be seen that different encountering positions of the trimaran with the freak wave crest can merely lead to slight difference (<5%) for the maximum peak-trough values of the heave and pitch motion, respectively.

To see the frequency-domain feature of the heave and pitch response, Figs. 15 and 16 show the comparison of the amplitude spectra of the heave and pitch time histories between different encountering positions of the trimaran at $V_m = 1.2$ m/s with the freak wave, respectively. It can

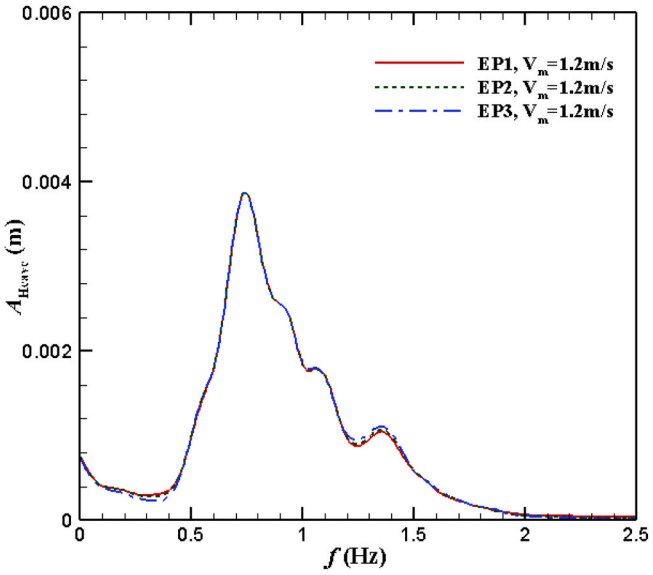

Fig. 15. Comparison of the amplitude spectra of the heave time histories of the trimaran encountering the freak wave with different positions at $V_m = 1.2$ m/s.

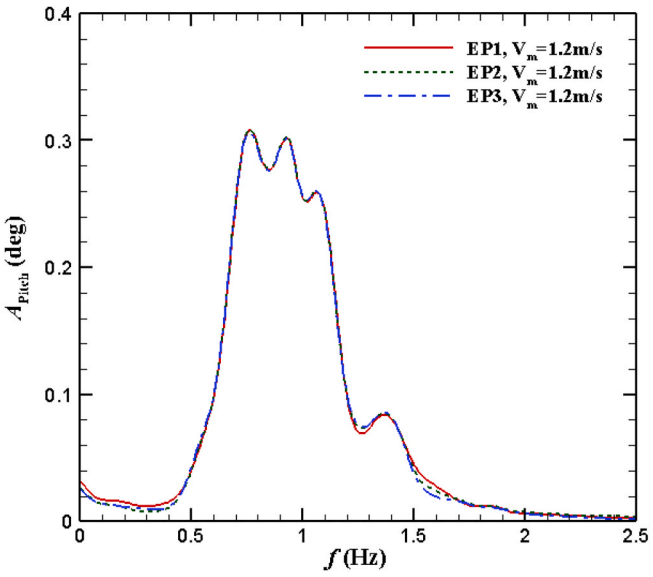

Fig. 16. Comparison of the amplitude spectra of the pitch time histories of the trimaran encountering the freak wave with different positions at $V_m = 1.2$ m/s.

be seen that there exist slight discrepancies of the amplitude spectra around higher and lower frequency range. In fact, the heave and pitch motions of the trimaran encountering a freak wave are transient. To observe the time-frequency characteristics of the transient heave and pitch motions of the trimaran encountering a freak wave, continuous wavelet transform (CWT) is adopted to obtain the wavelet time-frequency spectra of the motions. A complex Morlet wavelet with central frequency $f_c = 1$Hz and bandwidth parameter $f_b = 1$ is employed as a mother wavelet function. Figs. 17 and 18 show the comparison of the wavelet time-frequency spectra of the heave and pitch time histories of the trimaran encountering the freak wave with different positions at $V_m = 1.2$ m/s, respectively. It is observed in both figures that phase leading of the motion magnitudes around the occurrence time (60s) of the freak wave appears as the encountering position moves astern, which is consistent with the time histories of heave and pitch motions. It is also observed in Fig. 17 that the heave magnitudes with more high frequency

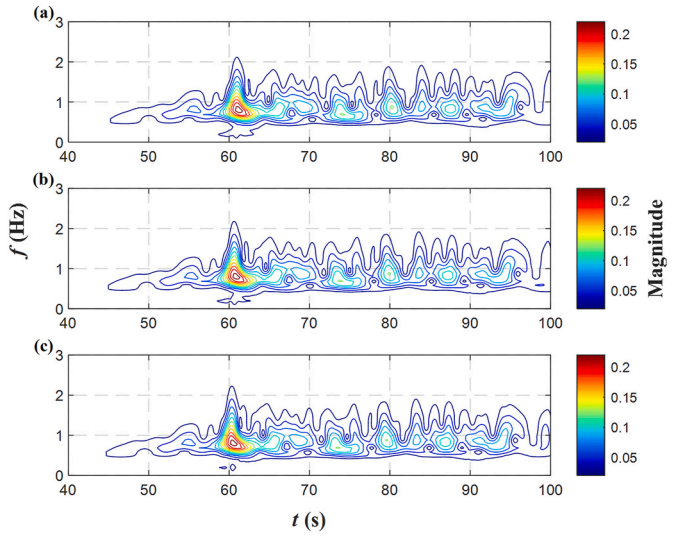

Fig. 17. Comparison of the wavelet time-frequency spectra of the heave time histories of the trimaran encountering the freak wave with different positions at $V_m = 1.2$ m/s: (a) EP1; (b) EP2; (c) EP3.

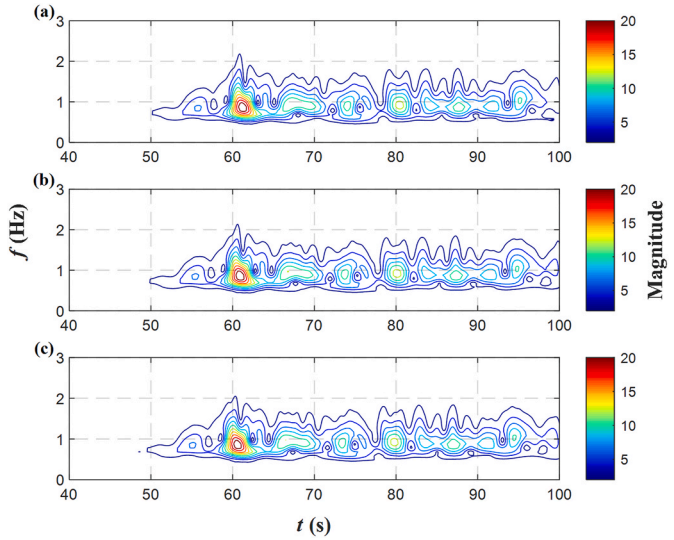

Fig. 18. Comparison of the wavelet time-frequency spectra of the pitch time histories of the trimaran encountering the freak wave with different positions at $V_m = 1.2$ m/s: (a) EP1; (b) EP2; (c) EP3.

components and less low frequency components around the occurrence time (60s) of the freak wave appear as the encountering position moves astern. While it is seen in Fig. 18 that the pitch magnitudes with less high frequency components around the occurrence time (60s) of the freak wave appear as the encountering position moves astern.

To further examine the influence of the encountering position of the trimaran at a higher forward speed with the freak wave crest on the motion response, Figs. 19 and 20 show the comparison of the time histories of the heave and pitch motion between different encountering positions of the trimaran at $V_m = 2.4$ m/s with the freak wave crest, respectively. It can be seen that the feature of phase leading of the heave and pitch time histories around the occurrence time (60s) of the freak wave as the encountering position moves astern is similar to that for the trimaran at the forward speed $V_m = 1.2$ m/s. Table 4 shows the comparison of the maximum peak-trough values of the heave and pitch time histories for the different encountering positions of the trimaran at the forward speed $V_m = 2.4$ m/s with the freak wave crest. It is also seen that

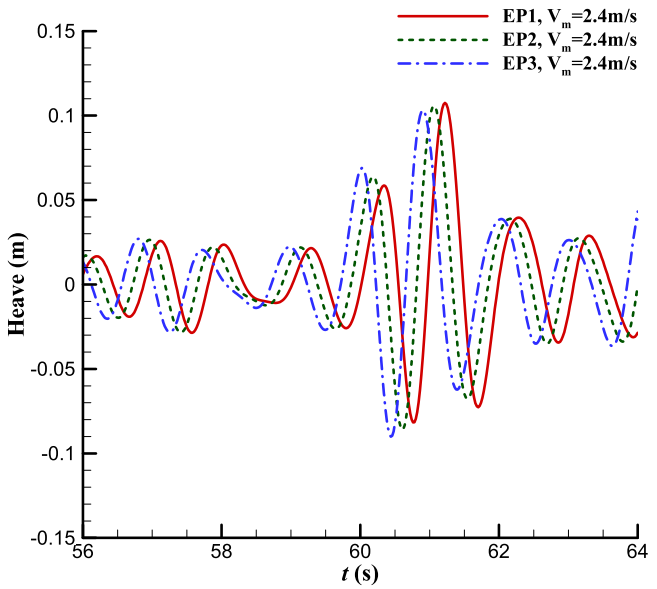

Fig. 19. Comparison of the time histories of the heave motion of the trimaran encountering the freak wave with different positions at $V_m = 2.4$ m/s.

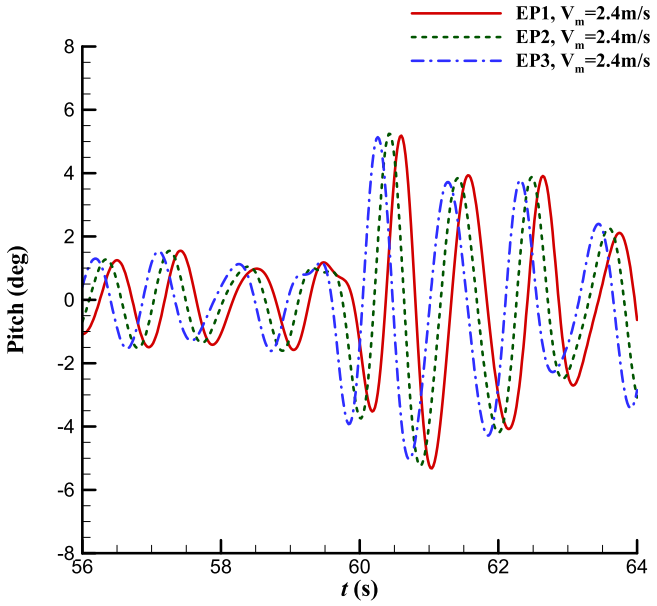

Fig. 20. Comparison of the time histories of the pitch motion of the trimaran encountering the freak wave with different positions at $V_m = 2.4$ m/s.

Table 4
Maximum peak-trough values of the heave and pitch time histories of the trimaran encountering the freak wave with different positions at $V_m = 2.4$ m/s.

Encountering position	Heave (m)	Pitch (deg)
EP1	0.1891	10.50
EP2	0.1915	10.48
EP3	0.1932	10.17

for the trimaran at a higher forward speed, different encountering positions still have slight influence on the maximum peak-trough values of the heave and pitch time histories.

Figs. 21 and 22 show the comparison of the amplitude spectra of the heave and pitch time histories between different encountering positions of the trimaran at $V_m = 2.4$ m/s with the freak wave, respectively. It is

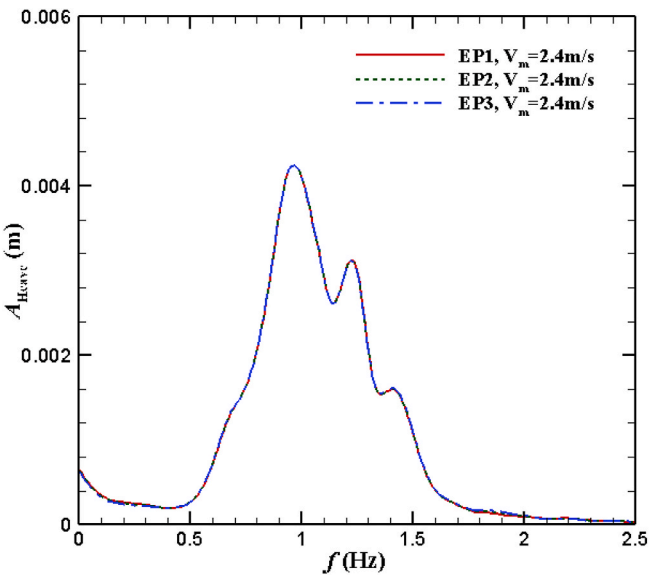

Fig. 21. Comparison of the amplitude spectra of the heave time histories of the trimaran encountering the freak wave with different positions at $V_m = 2.4$ m/s.

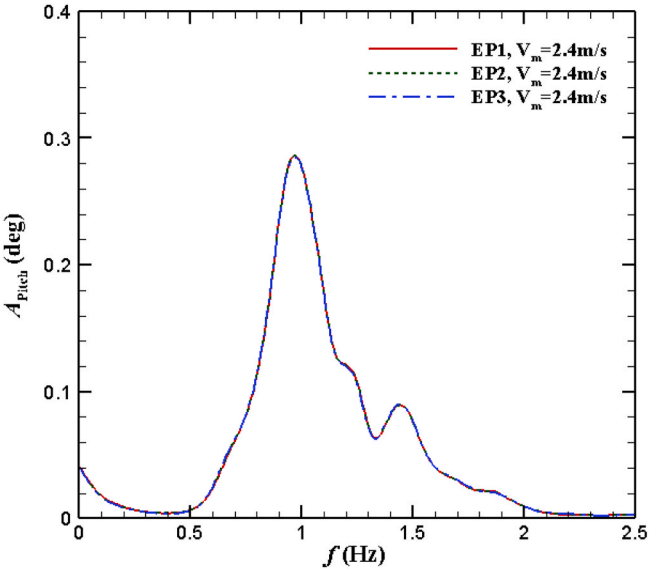

Fig. 22. Comparison of the amplitude spectra of the pitch time histories of the trimaran encountering the freak wave with different positions at $V_m = 2.4$ m/s.

clearly observed that the different encountering positions of the trimaran at a higher forward speed with the freak wave have almost no influence on the amplitude spectra. Figs. 23 and 24 show the comparison of the wavelet time-frequency spectra of the heave and pitch time histories of the trimaran encountering the freak wave with different positions at $V_m = 2.4$ m/s, respectively. It can be seen in both figures that all motion magnitudes appear to be more compact induced by the higher forward speed. Moreover, the trend of phase leading of the motion magnitudes can also be observed in the figures. The trend is not prominent due to the higher forward speed of the trimaran.

4.3. *Effect of forward speed*

In order to study the influence of forward speed of the trimaran on the motion response, the encountering position EP2 (CG) of the trimaran at different forward speeds ($V_m = 1.2$ m/s, 1.8 m/s and 2.4 m/s) with the

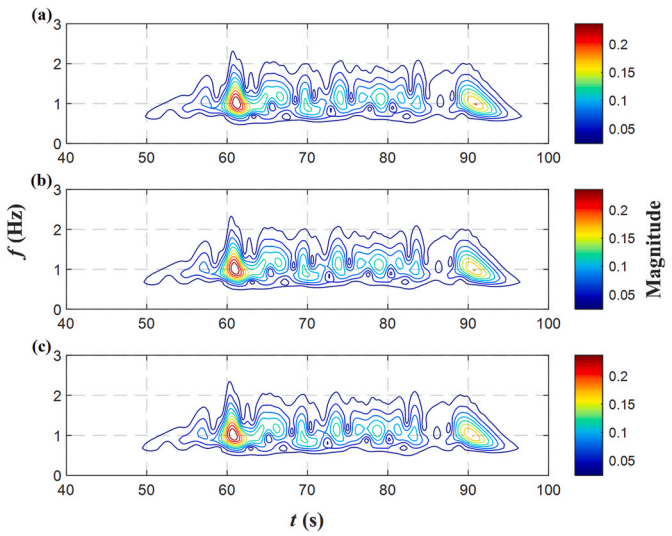

Fig. 23. Comparison of the wavelet time-frequency spectra of the heave time histories of the trimaran encountering the freak wave with different positions at V_m = 2.4 m/s: (a) EP1; (b) EP2; (c) EP3.

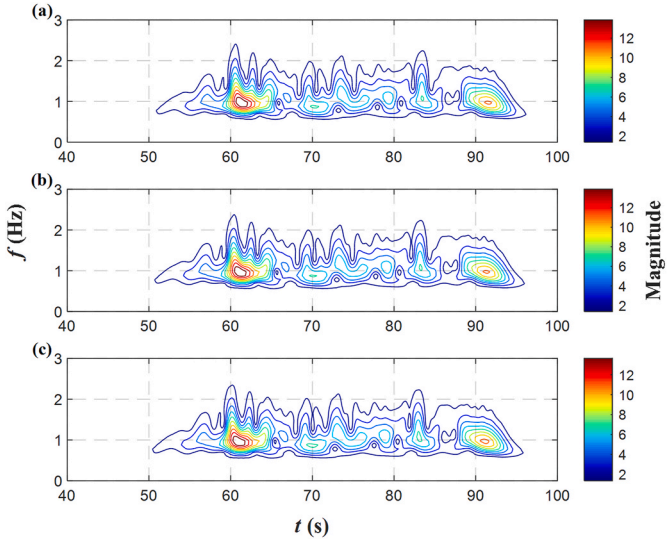

Fig. 24. Comparison of the wavelet time-frequency spectra of the pitch time histories of the trimaran encountering the freak wave with different positions at V_m = 2.4 m/s: (a) EP1; (b) EP2; (c) EP3.

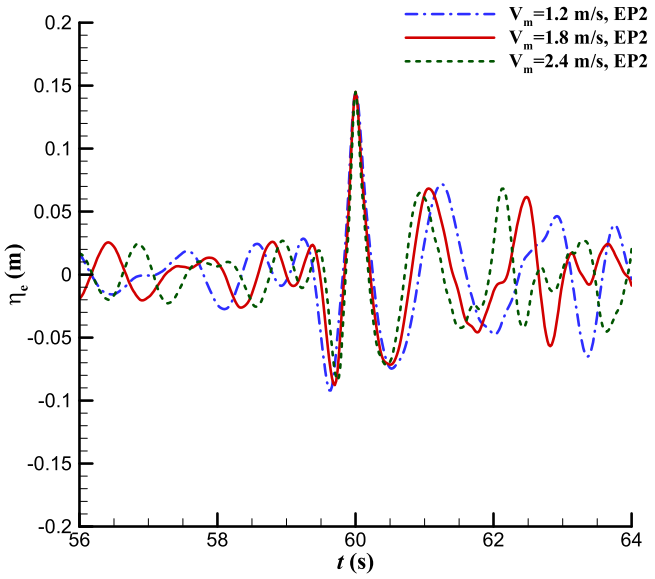

Fig. 25. Comparison of the encountered time histories of wave elevation by EP2 of the trimaran encountering the freak wave at different forward speeds.

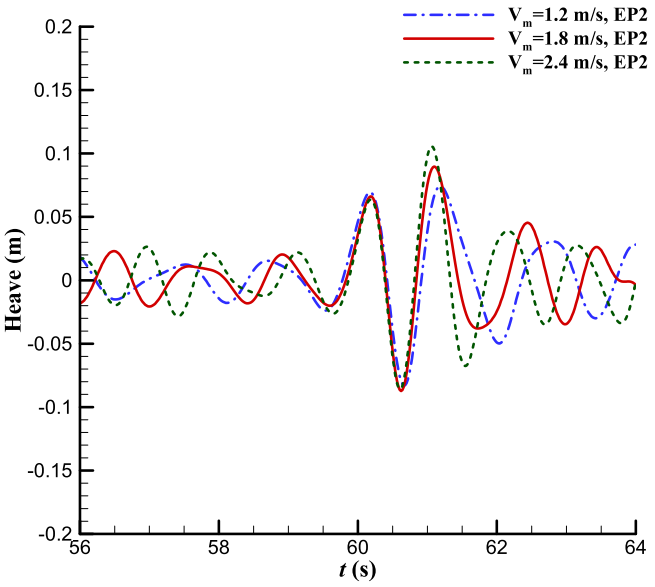

Fig. 26. Comparison of the time histories of the heave motion of the trimaran encountering the freak wave with EP2 at different forward speeds.

freak wave crest are considered in the numerical simulations. L1B1 layout of the trimaran is also considered in this subsection. Fig. 25 shows the comparison of the encountered time histories of wave elevation by EP2 of the trimaran encountering the freak wave at different forward speeds in the numerical simulations. It is clearly seen that the encountering wave elevation η_e at t = 60s is consistent for the trimaran with different forward speeds. This indicates that EP2 of the trimaran at different forward speeds rigorously encounters the freak wave crest at t = 60s. It is also demonstrated that the encountered time history of wave elevation for the trimaran at a higher forward speed appears to be condensed, which is consistent with the consensus that higher forward speeds of a travelling ship in head waves can lead to smaller encountered wave periods.

Figs. 26 and 27 show the comparison of the time histories of the heave and pitch motion of the trimaran encountering the freak wave crest with EP2 at different forward speeds (V_m = 1.2 m/s, 1.8 m/s and 2.4 m/s), respectively. It can be seen in Fig. 26 that the heave peak value around t = 61.5s increases evidently as the forward speed increases, while the pitch peak and trough values ranging from t = 60s to t = 62s decrease dramatically as the forward speed increases as shown in Fig. 27. To further see the influence of forward speed of the trimaran on the motion response magnitude, Table 5 shows the comparison of the maximum peak-trough values of the heave and pitch time histories of the trimaran encountering the freak wave crest with EP2 at different forward speeds. It can be clearly seen that the maximum peak-trough value of heave and pitch motion increases and decreases respectively as forward speed increases. This trend is consistent with that obtained by Bennett et al. (2013) based on experimental measurements and numerical simulations of a frigate travelling in abnormal waves as well as severe random seas. It is attributed to "tunnelling effect" of the frigate through a large amplitude wave observed in the experiments.

Figs. 28 and 29 shows the comparison of the amplitude spectra of the heave and pitch time histories of the trimaran encountering the freak

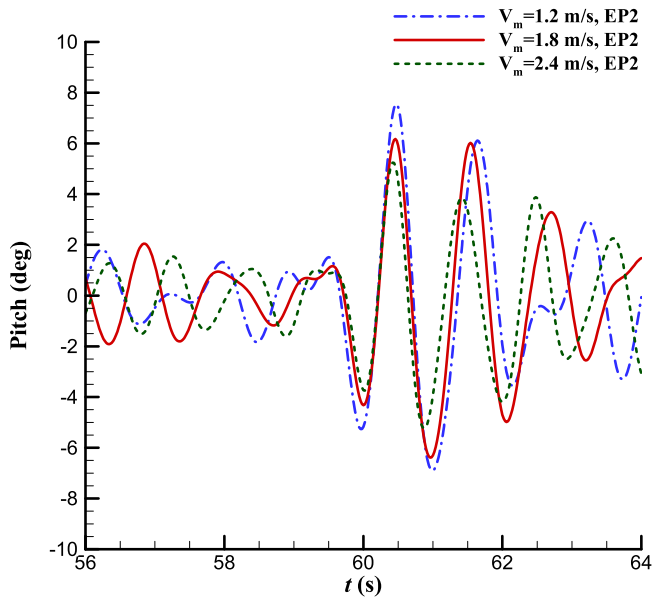

Fig. 27. Comparison of the time histories of the pitch motion of the trimaran encountering the freak wave with EP2 at different forward speeds.

Table 5
Maximum peak-trough values of the heave and pitch time histories of the trimaran encountering the freak wave with EP2 at different forward speeds.

Forward speed (m/s)	Heave (m)	Pitch (deg)
1.2	0.1571	14.45
1.8	0.1770	12.57
2.4	0.1915	10.48

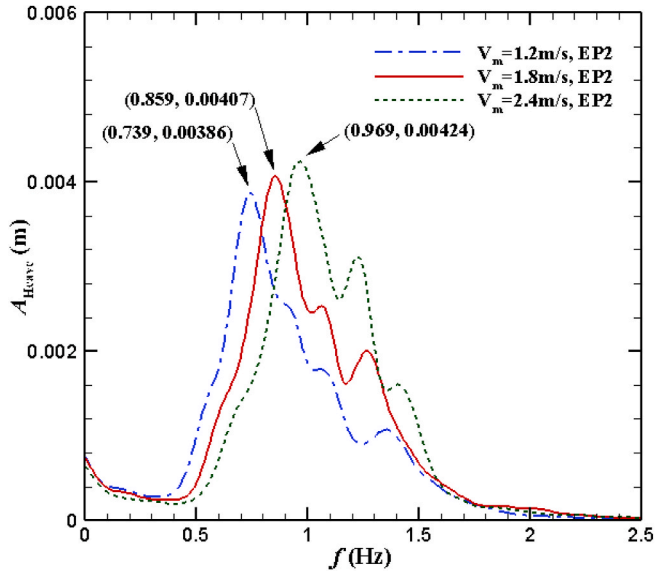

Fig. 28. Comparison of the amplitude spectra of the heave time histories of the trimaran encountering the freak wave with EP2 at different forward speeds.

wave with EP2 at different forward speeds, respectively. As shown in Fig. 28, the primary peak frequency and corresponding peak value of the heave motion spectrum increases from (0.739, 0.00386) to (0.969, 0.00424) as forward speed increases from 1.2 m/s to2.4 m/s. Moreover, it is also exhibited in Fig. 28 that more prominent high-frequency heave response spectral components arise with increased forward speed

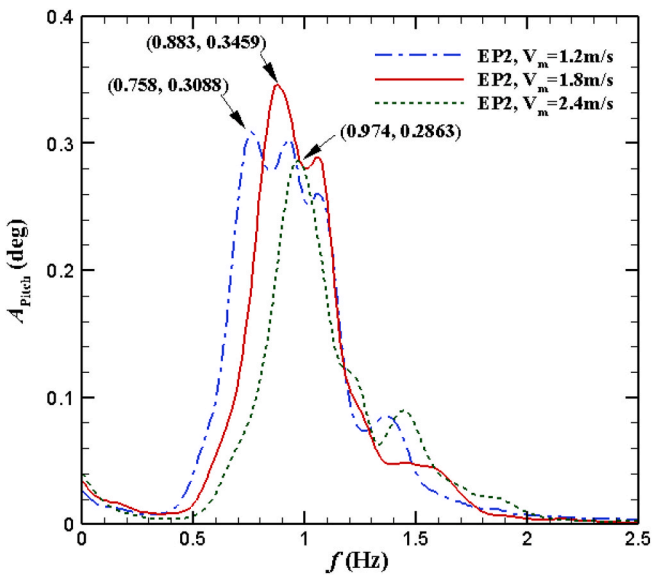

Fig. 29. Comparison of the amplitude spectra of the pitch time histories of the trimaran encountering the freak wave with EP2 at different forward speeds.

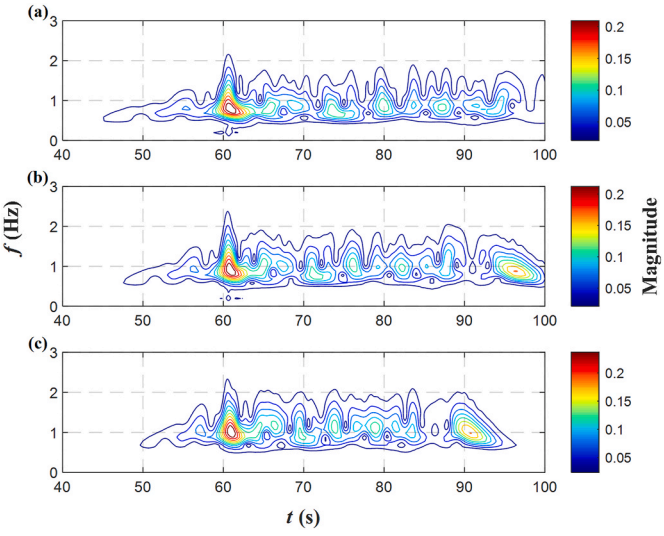

Fig. 30. Comparison of the wavelet time-frequency spectra of the heave time histories of the trimaran encountering the freak wave with EP2 at different forward speeds: (a) V_m = 1.2 m/s; (b) V_m = 1.8 m/s; (c) V_m = 2.4 m/s.

probably due to the interference effect between the main hull and side hulls. It is seen in Fig. 29 that only the primary peak frequency of the pitch response spectrum increases from 0.758 to 0.974 as forward speed increases from 1.2 m/s to 2.4 m/s. No more prominent high-frequency pitch motion components (>1Hz) arise with increased forward speed. It is noted that the area of the response spectral curve could be related to the statistical significant amplitude of the corresponding motion time history. The significant amplitude of pitch motion of the trimaran in the wave train containing the freak wave at V_m = 1.2 m/s, 1.8 m/s and 2.4 m/s is 7.29 deg, 7.36 deg and 5.75 deg, respectively. The is why the area of the pitch response spectral curve for the trimaran at V_m = 2.4 m/s appears to smaller than the others. This is mainly due to the trimaran at V_m = 2.4 m/s could approach a supercritical condition for pitch motion in terms of critical condition theory of ship motions that is elaborated in (Lewis, 1989).

Figs. 30 and 31 show the comparison of the wavelet time-frequency spectra of the heave and pitch time histories of the trimaran

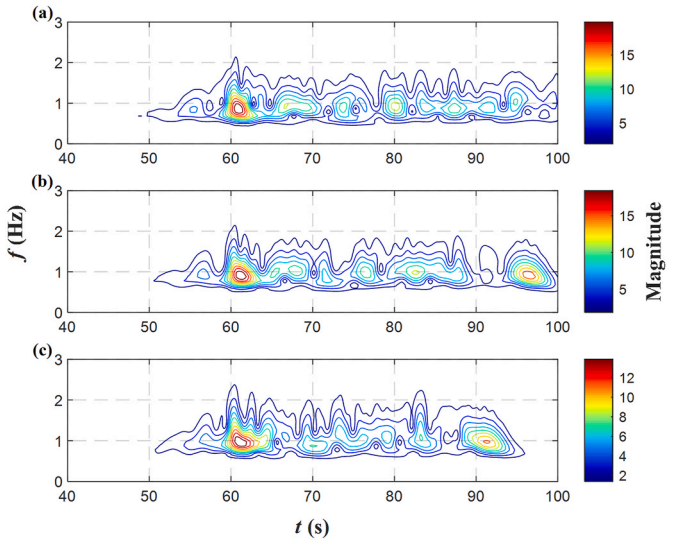

Fig. 31. Comparison of the wavelet time-frequency spectra of the pitch time histories of the trimaran encountering the freak wave with EP2 at different forward speeds: (a) $V_m = 1.2$ m/s; (b) $V_m = 1.8$ m/s; (c) $V_m = 2.4$ m/s.

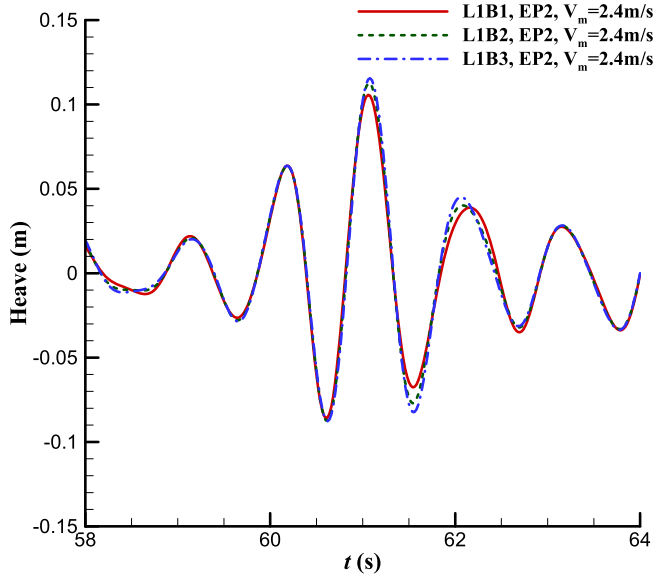

Fig. 32. Comparison of the time histories of the heave motion of the trimaran with different transverse layouts encountering the freak wave with EP2 at $V_m = 2.4$ m/s.

encountering the freak wave with EP2 at different forward speeds, respectively. It can be observed that as forward speed increases, the heave and pitch magnitudes with more high frequency components around the occurrence time (60s) of the freak wave appear, and the motion magnitudes appear to be more compact.

4.4. Effect of side-hull configuration

Many studies (Fang and Chen, 2008) (Gong et al., 2021) indicated that side-hull staggers and transverse spacings of a trimaran have significant effect on the motion characteristics in regular waves. It is of interest to study the influence of side-hull staggers and transverse spacings on the heave and pitch motion of the trimaran encountering with a freak wave crest. Figs. 32 and 33 show the comparison of the time histories of the heave and pitch motion for the trimaran with different transverse spacings at $V_m = 2.4$ m/s encountering with the freak wave

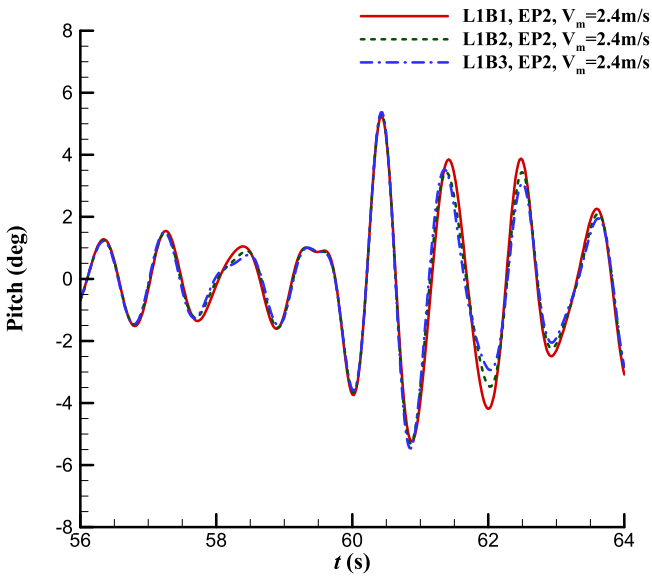

Fig. 33. Comparison of the time histories of the pitch motion of the trimaran with different transverse layouts encountering the freak wave with EP2 at $V_m = 2.4$ m/s.

Table 6
Maximum peak-trough values of the heave and pitch time histories of the trimaran with different transverse layouts encountering the freak wave with EP2 at $Vm = 2.4$ m/s.

Transverse layout	Heave (m)	Pitch (deg)
L1B1	0.1915	10.48
L1B2	0.2000	10.62
L1B3	0.2032	10.83

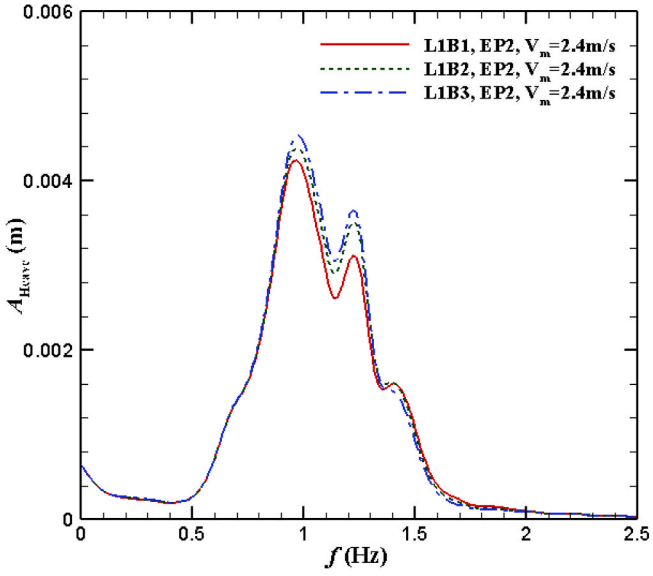

Fig. 34. Comparison of the amplitude spectra of the heave time histories of the trimaran with different transverse layouts encountering the freak wave with EP2 at $V_m = 2.4$ m/s.

crest with EP2, respectively. It can be seen that transverse spacings have slight influence on the maximum heave peak and trough values after the freak wave action, while almost have no influence on the maximum pitch peak and trough values. Table 6 shows the comparison of the maximum peak-trough values of the heave and pitch time histories for

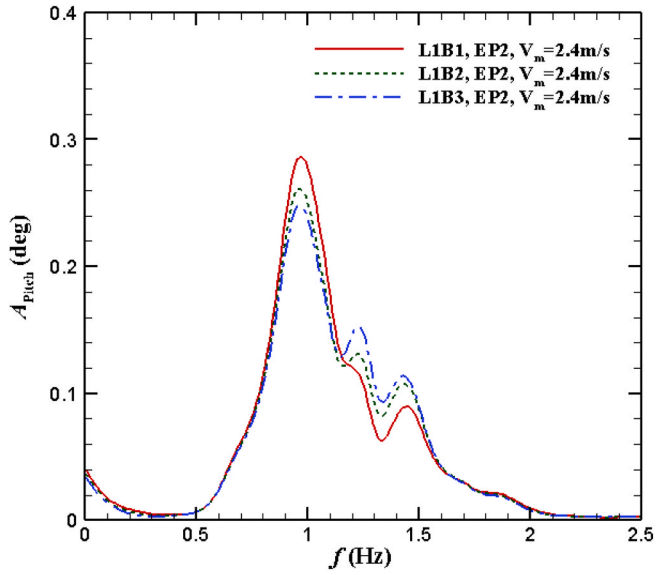

Fig. 35. Comparison of the amplitude spectra of the pitch time histories of the trimaran with different transverse layouts encountering the freak wave with EP2 at V_m = 2.4 m/s.

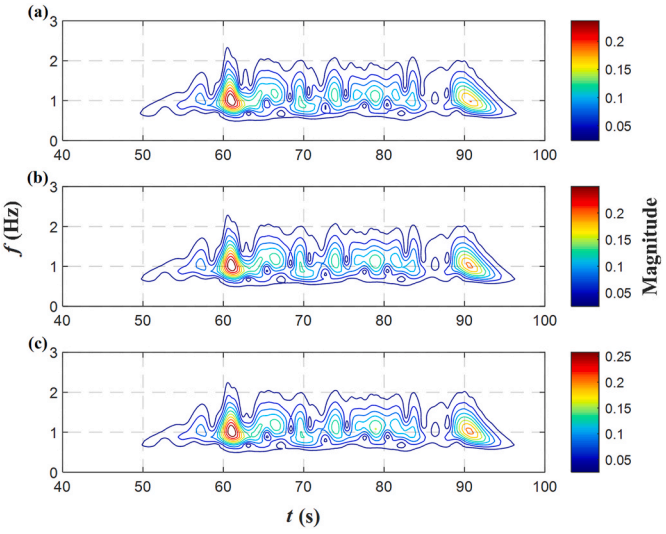

Fig. 36. Comparison of the wavelet time-frequency spectra of the heave time histories of the trimaran with different transverse layouts encountering the freak wave with EP2 at V_m = 2.4 m/s: (a) L1B1; (b) L1B2; (c) L1B3.

the trimaran with different transverse spacings at V_m = 2.4 m/s encountering with the freak wave crest. It is seen that as the transverse spacing increases, the maximum peak-trough value of the heave and pitch time histories slightly increases. This is mainly due to the interference between the main hull and side hulls weakens as the transverse spacing increases.

Figs. 34 and 35 show the comparison of the amplitude spectra of the heave and pitch time histories of the trimaran with different transverse layouts encountering the freak wave with EP2 at V_m = 2.4 m/s, respectively. It can be observed that the primary peak value around 1Hz of the heave amplitude spectrum increases as transverse spacing increases, while the primary peak value around 1Hz of the pitch amplitude spectrum decreases with increased transverse spacing. This means that the larger the transverse spacing is, the larger the heave response spectral values around the primary peak frequency and the smaller the pitch response spectral values around the primary peak frequency.

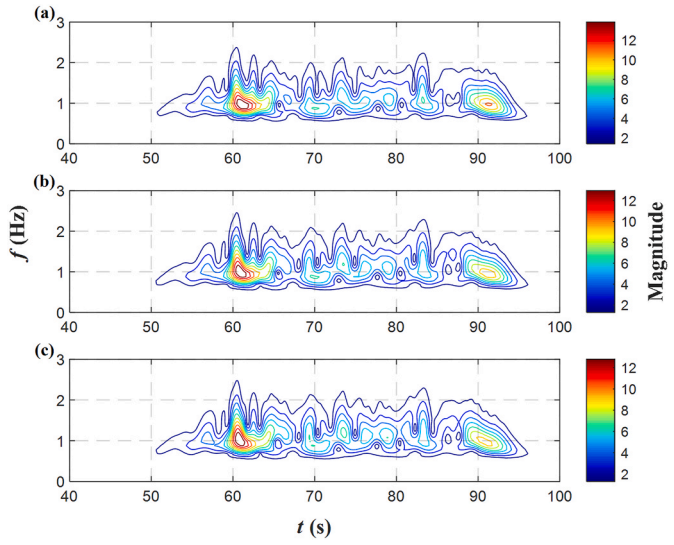

Fig. 37. Comparison of the wavelet time-frequency spectra of the pitch time histories of the trimaran with different transverse layouts encountering the freak wave with EP2 at V_m = 2.4 m/s: (a) L1B1; (b) L1B2; (c) L1B3.

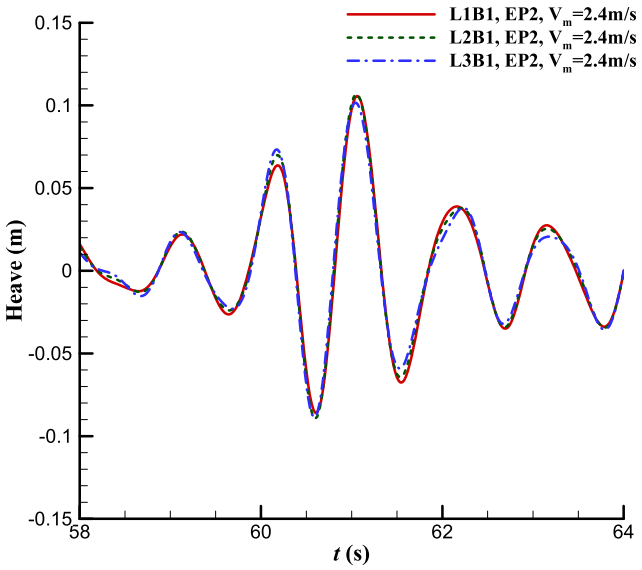

Fig. 38. Comparison of the time histories of the heave motion of the trimaran with different longitudinal layouts encountering the freak wave with EP2 at V_m = 2.4 m/s.

Figs. 36 and 37 show the comparison of the wavelet time-frequency spectra of the heave and pitch time histories of the trimaran with different transverse layouts encountering the freak wave with EP2 at V_m = 2.4 m/s, respectively. It is seen that as transverse spacing increases, the heave and pitch motion magnitudes with higher frequency components around the occurrence time (60s) of the freak wave appear to decrease and increase, respectively.

Figs. 38 and 39 show the comparison of the time histories of the heave and pitch motion for the trimaran with different staggers at V_m = 2.4 m/s encountering with the freak wave crest with EP2, respectively. It can be seen that side-hull staggers almost have no influence on the maximum heave peaks and troughs after the action with the freak wave crest. It is worth noting that the time history of pitch motion exhibits a whole downshift as the side hulls move forward. In fact, to merely consider hydrodynamic effects, the pitch radius of gyration remains constant in the numerical simulations. When the trimaran (EP2)

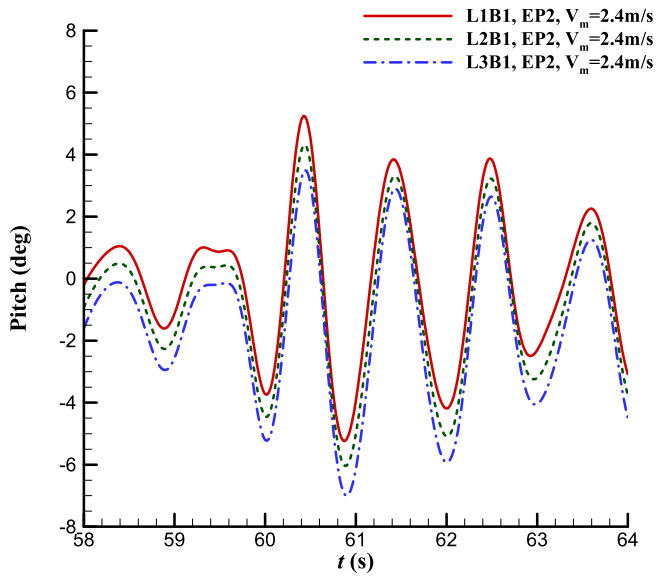

Fig. 39. Comparison of the time histories of the pitch motion of the trimaran with different longitudinal layouts encountering the freak wave with EP2 at V_m = 2.4 m/s.

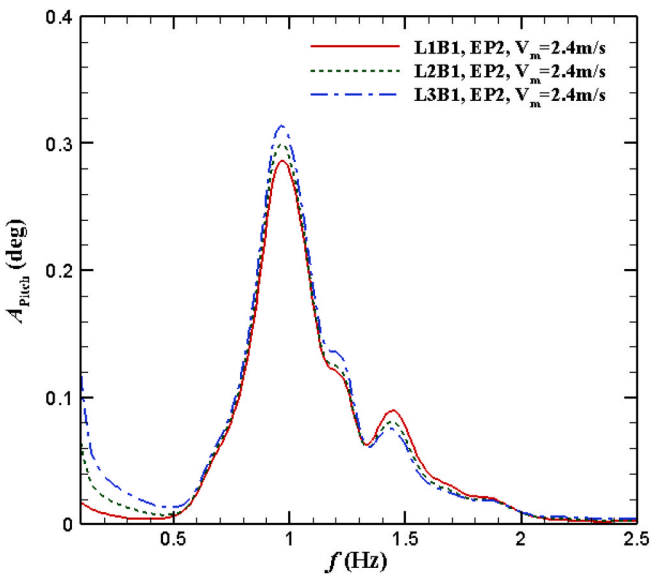

Fig. 41. Comparison of the amplitude spectra of the pitch time histories of the trimaran with different longitudinal layouts encountering the freak wave with EP2 at V_m = 2.4 m/s.

Table 7
Maximum peak-trough values of the heave and pitch time histories of the trimaran with different longitudinal layouts encountering the freak wave with EP2 at V_m = 2.4 m/s.

Longitudinal layout	Heave (m)	Pitch (deg)
L1B1	0.1915	10.48
L2B1	0.1962	10.36
L3B1	0.1902	10.51

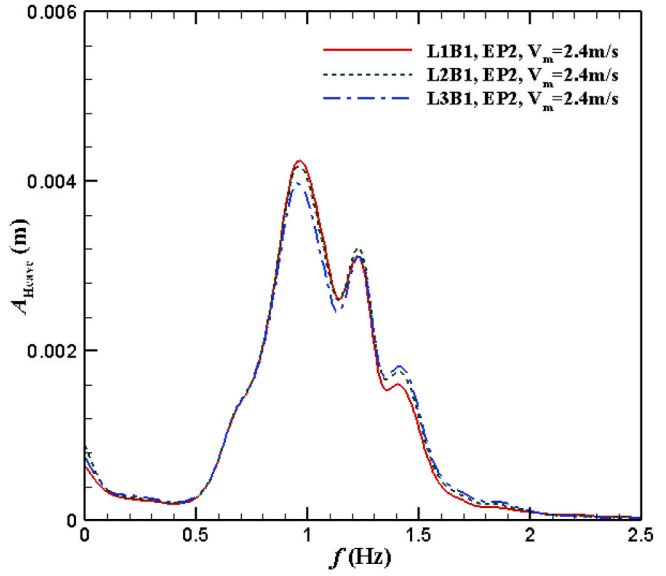

Fig. 40. Comparison of the amplitude spectra of the heave time histories of the trimaran with different longitudinal layouts encountering the freak wave with EP2 at V_m = 2.4 m/s.

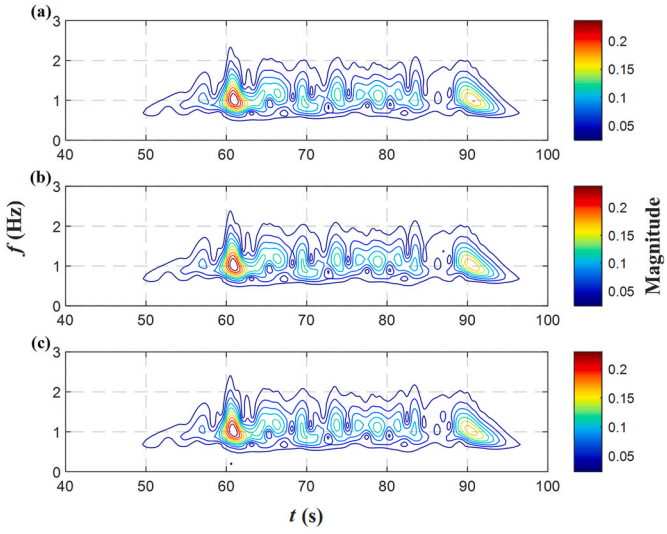

Fig. 42. Comparison of the wavelet time-frequency spectra of the heave time histories of the trimaran with different longitudinal layouts encountering the freak wave with EP2 at V_m = 2.4 m/s: (a) L1B1; (b) L2B1; (c) L3B1.

encounters the freak wave crest at t = 60s, the trimaran with more forward side hulls (L3B1) could suffer greater negative pitch moment in advance, inducing a larger negative pitch value at t = 60s for the trimaran with L3B1. As the freak wave crest propagates afterward, it would then lead to a smaller positive pitch value at t = 60.5s for the trimaran with L3B1 due to smaller positive pitch moment. Table 7 shows the comparison of the maximum peak-trough values of the heave and pitch time histories for the trimaran with different side-hull staggers at V_m = 2.4 m/s encountering with the freak wave crest. It is seen that the influence of side-hull staggers on the maximum peak-trough values of the heave and pitch time histories is rather slight.

Figs. 40 and 41 show the comparison of the amplitude spectra of the heave and pitch time histories of the trimaran with different longitudinal layouts encountering the freak wave with EP2 at V_m = 2.4 m/s, respectively. It can be seen that the primary peak value around 1Hz of heave amplitude spectrum decreases as L_h decreases, while the primary peak value around 1Hz of pitch amplitude spectrum increases with decreased L_h. This indicates that the more forward the side hulls are, the smaller the heave response spectral values around the primary peak frequency and the larger the pitch response spectral values around the primary peak frequency. Figs. 42 and 43 show the comparison of the

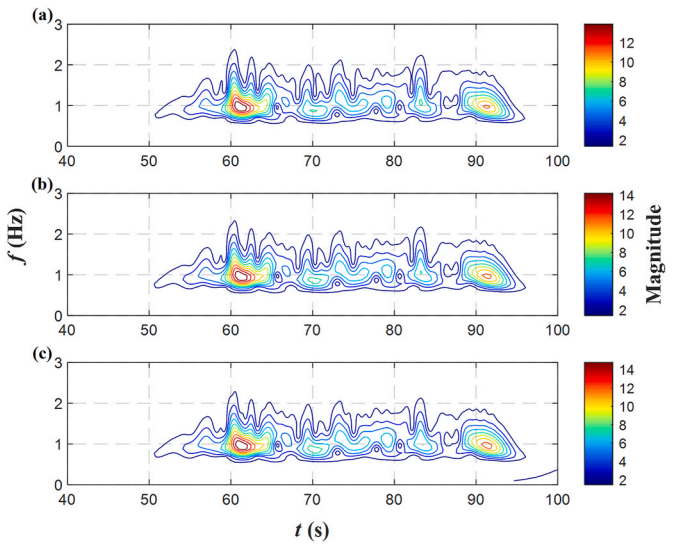

Fig. 43. Comparison of the wavelet time-frequency spectra of the pitch time histories of the trimaran with different longitudinal layouts encountering the freak wave with EP2 at $V_m = 2.4$ m/s: (a) L1B1; (b) L2B1; (c) L3B1.

wavelet time-frequency spectra of the heave and pitch time histories of the trimaran with different longitudinal layouts encountering the freak wave with EP2 at $V_m = 2.4$ m/s, respectively. It is observed that as the side hulls moves forward, the heave and pitch motion magnitudes with higher frequency components around the occurrence time (60s) of the freak wave appear to increase and decrease, respectively.

5. Conclusions

This study develops a hybrid frequency-time domain model to investigate motion characteristics of a travelling trimaran encountering a freak wave. Model test of the trimaran encountering a freak wave was carried out in a towing tank to validate the numerical model. The effect of the encountering position of the trimaran with the freak wave, the forward speed of the trimaran and the configuration of the side hulls on heave and pitch motions of the trimaran under the action of the freak wave were numerically studied. The main conclusions are drawn as follows.

(1) The agreement of the heave and pitch motion time histories of the travelling trimaran encountering a freak wave by numerical simulation and model test is generally satisfactory. The smaller experimental peaks and troughs are mainly due to the damping effect of the seaworthiness instrument in the test.

(2) It is found that there exists a feature of phase leading of the heave and pitch time histories around the occurrence time of the freak wave as the encountering position moves astern. The more ahead the action position of the freak wave crest, the later the time of the occurrence of the heave and pitch peaks and troughs. Different encountering positions of the trimaran with the freak wave crest can merely lead to slight difference for the maximum peak-trough values of the heave and pitch motion, respectively. The wavelet time-frequency spectra demonstrate that the heave magnitudes with more high frequency components and less low frequency components around the occurrence time (60s) of the freak wave appear as the encountering position moves astern, while the pitch magnitudes with less high frequency components around the occurrence time (60s) of the freak wave appear as the encountering position moves astern.

(3) It is found that the maximum peak-trough value of heave and pitch motion of the trimaran encountering the freak wave crest with EP2 at different forward speeds increases and decreases respectively as forward speed increases. A similar trend based on a frigate was also obtained by Bennett (Bennett et al., 2013) who attributed to "tunnelling effect" of the frigate through a large amplitude wave. It is shown that the primary peak frequency and corresponding peak value of the heave motion spectrum increases as forward speed increases, and more prominent high-frequency heave response spectral components arise with increased forward speed. It is indicated that only the primary peak frequency of the pitch response spectrum increases as forward speed increases. No more prominent high-frequency pitch motion spectral components (>1Hz) arise with increased forward speed. The smaller area of the pitch response spectral curve for the trimaran at $V_m = 2.4$ m/s , representing a smaller statistical significant amplitude of pitch motion, mainly due to the trimaran at $V_m = 2.4$ m/s could approach a supercritical condition. The wavelet time-frequency spectra indicate that as forward speed increases, the heave and pitch magnitudes with more high frequency components around the occurrence time (60s) of the freak wave appear, and the motion magnitudes appear to be more compact.

(4) As the transverse spacing increases, the maximum peak-trough value of the heave and pitch time histories slightly increases. It is found that the larger the transverse spacing is, the larger the heave response spectral values around the primary peak frequency and the smaller the pitch response spectral values around the primary peak frequency. The time history of pitch motion exhibits a whole downshift as the side hulls move forward. The influence of side-hull staggers on the maximum peak-trough values of the heave and pitch time histories is rather slight. It is demonstrated that the more forward the side hulls are, the smaller the heave response spectral values around the primary peak frequency and the larger the pitch response spectral values around the primary peak frequency. The wavelet time-frequency spectra reveal that as transverse spacing increases, the heave and pitch motion magnitudes with higher frequency components around the occurrence time (60s) of the freak wave appear to decrease and increase, respectively. While as the side hulls moves forward, the heave and pitch motion magnitudes with higher frequency components around the occurrence time (60s) of the freak wave appear to increase and decrease, respectively.

In this study, the freak wave train in time-domain numerical simulations is generated through linear superposition of component waves. Nonlinear wave models will be considered to generate freak waves in future studies.

CRediT authorship contribution statement

Zhen Liu: Writing – review & editing, Writing – original draft, Visualization, Validation, Project administration, Methodology, Investigation, Funding acquisition, Formal analysis, Data curation, Conceptualization. **Haipeng Zhang:** Validation, Investigation, Formal analysis. **Lei Shi:** Validation, Investigation, Formal analysis. **Kaiyuan Shi:** Validation, Methodology. **Gang Chen:** Writing – review & editing, Supervision, Resources, Funding acquisition, Conceptualization. **Longbin Tao:** Writing – review & editing, Writing – original draft, Supervision, Methodology, Investigation, Formal analysis, Conceptualization.

Declaration of competing interest

The authors declare that they have no known competing financial interests or personal relationships that could have appeared to influence the work reported in this paper.

Acknowledgements

This study is partially supported by National Natural Science Foundation of China (Grant no. 52271335). The authors would like to appreciate the financial support.

References

Acanfora, M., Montewka, J., Hinz, T., Matusiak, J., 2017. Towards realistic estimation of ship excessive motions in heavy weather. A case study of a containership in the Pacific Ocean. Ocean. Eng. 138, 140–150. https://doi.org/10.1016/j.oceaneng.2017.04.025.

Begovic, E., Bertorello, C., Cakici, F., Kahramanoglu, E., Rinauro, B., 2020. Vertical motions prediction in irregular waves using a time domain approach for hard chine displacement hull. J. Mar. Sci. Eng. 8. https://doi.org/10.3390/jmse8050337.

Bennett, S.S., Hudson, D.A., Temarel, P., 2013. The influence of forward speed on ship motions in abnormal waves: experimental measurements and numerical predictions. J. Fluid Struct. 39, 154–172. https://doi.org/10.1016/J.JFLUIDSTRUCTS.2013.01.006.

Bertotti, L., Cavaleri, L., 2008. The predictability of the "Voyager" accident. Nat. Hazards Earth Syst. Sci. 8, 533–537. https://doi.org/10.5194/nhess-8-533-2008.

Clauss, G.F., Klein, M., 2011. The New Year Wave in a seakeeping basin: generation, propagation, kinematics and dynamics. Ocean. Eng. 38, 1624–1639. https://doi.org/10.1016/J.OCEANENG.2011.07.022.

Colagrossi, A., Lugni, C., Landrini, M., Graziani, G., 2001. Numerical and experimental transient tests for ship seakeeping. Int. J. Offshore Polar Eng. 11.

Cummins, W.E., 1962. The Impulse Response Function and Ship Motions. Washington DC.

Deng, R., Luo, F., Wu, T., Chen, S., Li, Y., 2019. Time-domain numerical research of the hydrodynamic characteristics of a trimaran in calm water and regular waves. Ocean. Eng. 194, 106669. https://doi.org/10.1016/J.OCEANENG.2019.106669.

Duan, W.Y., Wang, S.M., Ma, S., 2019. Verification of application of the 2.5D method in high-speed trimaran vertical motion and added resistance prediction. Ocean. Eng. 187, 106177. https://doi.org/10.1016/J.OCEANENG.2019.106177.

Faltinsen, O.M., 2005. Hydrodynamics of High-Speed Marine Vehicles. Cambridge University Press.

Fang, M.C., Chen, T.Y., 2008. A parametric study of wave loads on trimaran ships traveling in waves. Ocean. Eng. 35, 749–762. https://doi.org/10.1016/J.OCEANENG.2008.02.001.

Fang, M.-C., Too, G.-Y., 2006. The effect of side hull arrangements on the motions of the trimaran ship in waves. Nav. Eng. J. 118, 27–37.

Gong, J., Yan, S., Ma, Q., Li, Y., 2020. Added resistance and seakeeping performance of trimarans in oblique waves. Ocean. Eng. 216, 107721. https://doi.org/10.1016/j.oceaneng.2020.107721.

Gong, J., Li, Y., Cui, M., Fu, Z., Hong, Z., 2021. The effect of side-hull position on the seakeeping performance of a trimaran at various headings. Ocean. Eng. 239, 109897. https://doi.org/10.1016/J.OCEANENG.2021.109897.

Guedes Soares, C., Fonseca, N., Pascoal, R., Clauss, G.F., Schmittner, C.E., Hennig, J., 2005. Analysis of Design wave loads on an FPSO accounting for abnormal waves. J. Offshore Mech. Arctic Eng. 128, 241–247. https://doi.org/10.1115/1.2166656.

Haver, S., Andersen, O.J., 2000. Freak waves: rare realizations of a typical population or typical realizations of a rare population? ISOPE International Ocean and Polar Engineering Conference ISOPE–I.

Hebblewhite, K., Sahoo, P.K., Doctors, L.J., 2007. A case study: theoretical and experimental analysis of motion characteristics of a trimaran hull form. Ships Offshore Struct. 2, 149–156. https://doi.org/10.1080/17445300701430242.

Kharif, C., Pelinovsky, E., 2003. Physical mechanisms of the rogue wave phenomenon. Eur. J. Mech. B Fluid 22, 603–634. https://doi.org/10.1016/j.euromechflu.2003.09.002.

Kharif, C., Pelinovsky, E., Slunyaev, A., 2008. Rogue Waves in the Ocean. Springer Science \& Business Media.

King, B.K., 1987. Time-domain Analysis of Wave Exciting Forces on Ships and Bodies.

Kriebel, D.L., Alsina, M.V., 2000. Simulation of extreme waves in a background random sea. ISOPE International Ocean and Polar Engineering Conference, pp. ISOPE–I.

Lewis, E.V., 1989. Principles of Naval Architecture: Volume III. Motions in Waves and Controllability. SNAME.

Liang, H., Ren-chuan, Z., Guo-ping, M., Ju, F., 2016. Study on Havelock form translating–pulsating source Green's function distributing on horizontal line segments and its applications. Ocean. Eng. 124, 306–323. https://doi.org/10.1016/J.OCEANENG.2016.07.056.

Pennino, S., Scamardella, A., 2023. Motions assessment using a time domain approach for a research ship in antarctic waters. J. Mar. Sci. Eng. 11. https://doi.org/10.3390/jmse11030558.

Tang, H., Ren, H., Yu, P., Tian, B., 2020. Experimental investigation of seakeeping performance and load response of trimaran in small heeling condition. Appl. Ocean Res. 101, 102275. https://doi.org/10.1016/J.APOR.2020.102275.

Wei, Y., 2007. Research of Multi-Hull Vessels' Longitudinal Motion Prediction. Harbin Engineering University.

Yao, C., Dong, G., Sun, X.S., Zheng, Y., Feng, D., 2023. Numerical study on motion and added resistance of a trimaran advancing in waves based on hybrid Green function method. Appl. Ocean Res. 130, 103432. https://doi.org/10.1016/J.APOR.2022.103432.

Yu, Y., 2003. Random Wave and its Applications to Engineering. Dalian University of Technology Press.

Zhang, H., Cui, J., Shi, H., Guedes Soares, C., 2022. Analysis of the peaks of ship motions in linear and nonlinear focused waves. Ocean. Eng. 266, 113028. https://doi.org/10.1016/J.OCEANENG.2022.113028.

Zhang, Y., Hu, J., Ma, S., Wang, P., 2023. Anti-rolling analysis and resistance optimization of a new anti-rolling hydrofoil for the trimaran vessel. Ocean. Eng. 272, 113837. https://doi.org/10.1016/J.OCEANENG.2023.113837.